

RESEARCH ARTICLE

10.1002/2014JD022067

Key Points:

- CH₄ and N₂O kinetic and photochemical uncertainties are updated
- Uncertainty ranges in the global lifetimes of CH₄ and N₂O are reduced
- CH₄ and N₂O loss uncertainties significantly impact global ozone

Correspondence to:

E. L. Fleming, and J. B. Burkholder,
eric.l.fleming@nasa.gov;
James.B.Burkholder@noaa.gov

Citation:

Fleming, E. L., et al. (2015), The impact of current CH₄ and N₂O atmospheric loss process uncertainties on calculated ozone abundances and trends, *J. Geophys. Res. Atmos.*, 120, 5267–5293, doi:10.1002/2014JD022067.

Received 30 MAY 2014

Accepted 17 APR 2015

Accepted article online 21 APR 2015

Published online 29 MAY 2015

The impact of current CH₄ and N₂O atmospheric loss process uncertainties on calculated ozone abundances and trends

Eric L. Fleming^{1,2}, Christian George³, Dwayne E. Heard⁴, Charles H. Jackman¹, Michael J. Kurylo⁵, Wahid Mellouki⁶, Vladimir L. Orkin⁷, William H. Swartz⁸, Timothy J. Wallington⁹, Paul H. Wine¹⁰, and James B. Burkholder¹¹

¹NASA Goddard Space Flight Center, Greenbelt, Maryland, USA, ²Science Systems and Applications, Inc, Lanham, Maryland, USA, ³Centre National de la Recherche Scientifique, IRCELYON, CRNS, University Claude Bernard, Lyon, France, ⁴School of Chemistry, University of Leeds, Leeds, UK, ⁵Goddard Earth Sciences, Technology, and Research Program, Universities Space Research Association, Greenbelt, Maryland, USA, ⁶Institut de Combustion, Aérothermique, Réactivité et Environnement, CNRS, Orléans CEDEX02, France, ⁷National Institute of Standards and Technology, Gaithersburg, Maryland, USA, ⁸Applied Physics Laboratory, Johns Hopkins University, Laurel, Maryland, USA, ⁹Systems Analytics and Environmental Sciences Department, Ford Motor Company, Dearborn, Michigan, USA, ¹⁰School of Chemistry and Biochemistry and School of Earth and Atmospheric Sciences, Georgia Institute of Technology, Atlanta, Georgia, USA, ¹¹Earth System Research Laboratory, Chemical Sciences Division, National Oceanic and Atmospheric Administration, Boulder, Colorado, USA

Abstract The atmospheric loss processes of N₂O and CH₄, their estimated uncertainties, lifetimes, and impacts on ozone abundance and long-term trends are examined using atmospheric model calculations and updated kinetic and photochemical parameters and uncertainty factors from Stratospheric Processes and their Role in Climate (SPARC) (2013). The uncertainty ranges in calculated N₂O and CH₄ global lifetimes computed using the SPARC estimated uncertainties are reduced by nearly a factor of 2 compared with uncertainties from Sander et al. (2011). Uncertainties in CH₄ loss due to reaction with OH and O(¹D) have relatively small impacts on present-day global total ozone (±0.2–0.5%). Uncertainty in the Cl + CH₄ reaction affects the amount of chlorine in radical versus reservoir forms and has a modest impact on present-day southern hemisphere (SH) polar ozone (~±6%) and on the rate of past ozone decline and future recovery. Uncertainty in the total rate coefficient for the O(¹D) + N₂O reaction results in a substantial range in present-day stratospheric odd nitrogen (±20–25%) and global total ozone (±1.5–2.5%). Uncertainty in the O(¹D) + N₂O reaction branching ratio for the O₂ + N₂ and 2NO product channels results in moderate impacts on odd nitrogen (±10%) and global ozone (±1%), with uncertainty in N₂O photolysis resulting in relatively small impacts (±5% in odd nitrogen, ±0.5% in global ozone). Uncertainties in the O(¹D) + N₂O reaction and its branching ratio also affect the rate of past global ozone decline and future recovery, with a range in future ozone projections of ±1–1.5% by 2100, relative to present day.

1. Introduction

Methane (CH₄) and nitrous oxide (N₂O) are key atmospheric trace gases that impact stratospheric ozone abundances and radiative forcing of the atmosphere. N₂O is a long-lived (well-mixed) atmospheric trace species with an estimated steady state lifetime of 123 years [*Stratospheric Processes and their Role in Climate (SPARC)*, 2013]. N₂O is primarily removed from the atmosphere via chemical reaction and photodissociation in the stratosphere. Oxidation of N₂O, primarily via the O(¹D) + N₂O reaction, leads to the formation of NO and is the dominant source (~90%) of stratospheric NO_x (NO_x = NO + NO₂) and total odd nitrogen NO_y (NO_y = N + NO + NO₂ + NO₃ + 2 N₂O₅ + HONO + HNO₃ + HO₂NO₂ + ClONO₂ + BrONO₂) [Vitt and Jackman, 1996]. Stratospheric NO_x is important because it impacts the stratospheric ozone abundance through its involvement in catalytic ozone destruction cycles, null cycles, and reservoir formation [Crutzen, 1970; Crutzen, 1971; Brasseur and Solomon, 2005]. Following the implementation of the Montreal protocol (and its amendments and adjustments) and the subsequent decline of atmospheric chlorofluorocarbons, N₂O has become the most significant substance that depletes ozone

and the third most important greenhouse gas (GHG), following CO₂ and CH₄, that is emitted into the atmosphere. N₂O is, however, currently not regulated under international agreements [United Nations Environment Programme, 2013].

CH₄ is also considered a long-lived trace gas, although its atmospheric lifetime of ~10 years is much less than that of N₂O. CH₄ is removed primarily by reaction with the OH radical in the troposphere, with a tropospheric partial lifetime of 10.2–11.2 years as estimated from the interpretation of global observations [Prinn *et al.*, 2005; Prather *et al.*, 2012]. The methane lifetime for loss in the stratosphere is 150–160 years as computed in this work and other models [SPARC, 2013]. The atmospheric chemistry of CH₄ impacts ozone globally in several ways [e.g., see Brasseur and Solomon, 2005]. The Cl + CH₄ → HCl + CH₃ reaction is a minor loss process for CH₄ but represents an important sink for reactive chlorine in the stratosphere, thereby reducing chlorine catalyzed ozone loss. The reactive loss of CH₄ also impacts the stratospheric HO_x (HO_x = OH + HO₂) budget and represents a significant source of stratospheric H₂O. Furthermore, CH₄ has a significant impact on the radiative forcing of the atmosphere, both directly as a greenhouse gas and indirectly via its reactive loss, which leads to the production of tropospheric ozone and stratospheric H₂O.

An accurate understanding of the atmospheric processing of CH₄ and N₂O is an essential element in model calculations of stratospheric ozone and its recovery and of atmospheric radiative forcing. Current chemistry-climate models show a wide range of calculated long-term ozone changes, with a range of as much as 20–30 Dobson units (DU) in annual mean total ozone at midlatitudes during 1960–2100 [WMO, 2011]. This range is mainly due to the individual model treatment of dynamics, chemistry, photolysis, and other processes. There is also uncertainty in calculated ozone due to uncertainty in the input parameters that are common among models, and such uncertainty is not necessarily represented in the range of model ozone calculations. Model input includes kinetic and photochemical parameters that are primarily obtained from critical evaluations of laboratory studies [Atkinson *et al.*, 2008; Sander *et al.*, 2011; SPARC, 2013]. A few model studies have analyzed the ozone impacts due to uncertainties in these input parameters, primarily focusing on partitioning reactions [e.g., Considine *et al.*, 1999; Kawa *et al.*, 2009]. However, quantification of uncertainties in the kinetic and photochemical inputs for source gas losses, and the impacts on calculated lifetimes and ozone abundance, are important elements of modeling that are often unaccounted for.

The SPARC [2013] lifetime report addressed atmospheric lifetimes and uncertainties derived from observational data and modeling for a number of key ozone depleting substances (ODSs), their replacements, and related species, including CH₄ and N₂O. The modeling efforts used in that report are discussed further in a recent paper by Chipperfield *et al.* [2014]. The SPARC report included a critical evaluation of the kinetic and photochemical loss processes of ODSs and related species, along with their estimated uncertainties. The loss processes include OH, O(¹D), and Cl atom reactions and photochemical removal via Lyman- α and UV photolysis. The relative importance and impacts of these loss processes were evaluated using the NASA/Goddard Space Flight Center (GSFC) two-dimensional (2-D) model. Based solely on the estimated 2 σ uncertainties in the kinetic and photochemical parameters, the lifetime uncertainties (i.e., the range of possible calculated lifetimes) were estimated for CH₄ (9.8 ± 1.2 years, ±13%) and N₂O (123 ± 7 years, ±5.7%).

The SPARC [2013] report briefly investigated the impact of loss uncertainties on ozone. Overall, the kinetic and photochemical parameter uncertainties for the halogenated ODSs were found to have a minor effect on calculated total ozone. However, uncertainties in the CH₄ and N₂O losses were shown to have significant impacts on calculated ozone [see SPARC, 2013, Chapter 3] and require further attention. For example, even though only a small amount (~6%) of N₂O loss produces odd nitrogen, via reaction with O(¹D), uncertainty in this loss can substantially affect stratospheric NO_x and ozone.

In this work, the GSFC 2-D model is used to investigate the range in calculated lifetimes, the stratospheric ozone abundance, and its long-term trends (1960–2100) based on the estimated uncertainties in the kinetic and photochemical loss processes for CH₄ and N₂O. The following sections describe (i) an overview of the SPARC [2013] approaches and evaluation of the CH₄ and N₂O kinetic and photochemical parameters and their uncertainties, (ii) the GSFC 2-D model and the methodology used to evaluate the impacts on

calculated atmospheric lifetimes and ozone, and (iii) the model results including an evaluation of the impacts of the individual loss processes and their uncertainties, as well as the resulting total calculated global ozone uncertainty. We also examine the sensitivity of the ozone impacts to future greenhouse gas (GHG) scenarios. The Global Modeling Initiative (GMI) three-dimensional (3-D) chemistry and transport model (CTM) was used along with the 2-D model to evaluate the present-day ozone response to the Cl + CH₄ reaction uncertainty in the polar region.

2. Kinetic and Photochemical Data Evaluation

In this section, a brief overview of the methodologies used in the SPARC [2013] kinetic and photochemical parameter evaluation and a summary of the recommendations for the OH, O(¹D), and Cl gas-phase reaction rate coefficients, k , and their temperature dependences, and of the vacuum ultraviolet/ultraviolet (VUV/UV) absorption spectra for CH₄ and N₂O is given. Other gas-phase loss processes such as reaction with other atmospheric oxidants, e.g., the NO₃ radical and O₃, are minor atmospheric processes for CH₄ and N₂O and are not considered further in this paper. The specific kinetic and photochemical details relating to the atmospheric chemistry of CH₄ and N₂O are presented in separate subsections below. Summaries of the evaluations of the other compounds that were included in the SPARC report are available in the supporting information of Chapter 3 at the SPARC website (<http://www.sparc-climate.org/publications/sparc-reports/sparc-report-no6/>). For the compounds considered in the SPARC report, the recommendations given build on those given in the NASA/Jet Propulsion Laboratory (JPL) Panel for Data Evaluation, "Chemical Kinetics and Photochemical Data for Use in Atmospheric Studies" [Sander *et al.*, 2011] (herein referred to as JPL10-6) and the International Union of Pure and Applied Chemistry (IUPAC) Subcommittee for Gas Kinetic Data Evaluation [Atkinson *et al.*, 2008] (herein referred to as IUPAC).

SPARC [2013] recommendations for the reaction rate coefficients, $k(T)$, for the OH radical, O(¹D) atom, and Cl atom reactions were based on a comprehensive evaluation/consideration of all available laboratory data for these reactions (note that not all studies were included in deriving the final recommendations). In most cases, under atmospheric conditions, the reactions proceed via simple direct abstraction mechanisms, and the reaction rate coefficient temperature dependence was parameterized using an Arrhenius equation $k(T) = A \times \exp(-E/RT)$, where the preexponential, A , and activation energy, E , parameters are variables in a least squares fitting of experimental data. In obtaining the optimized E value from multiple independent studies, the results from the individual studies were scaled to the recommended value for the 298 K rate coefficient before performing a global fit. In many cases, experimental rate coefficient data for a reaction were available at temperatures higher than commonly found in the atmosphere. The experimental data obtained at higher temperatures, although not directly applicable to atmospheric chemistry, can often provide valuable constraints on the Arrhenius fitting and extrapolation to lower temperatures as well as the identification of non-Arrhenius (curvature) behavior. Non-Arrhenius behavior has been observed in both the Cl and OH reactions with CH₄ and is discussed further below. In many cases, direct measurements of reaction rate coefficients are not available at the lowest temperatures observed in the atmosphere (~190 K) primarily due to the limitations of the experimental methods used. This places additional emphasis on the ability to reliably extrapolate rate coefficient data to lower temperatures. Arrhenius plots for the OH and Cl reactions with CH₄ and the O(¹D) reaction with CH₄ and N₂O are given in Figures 1–4.

For trace gases with extremely low reactivity, it is difficult to experimentally measure the true reaction rate coefficient, and upper limits to the rate coefficients are often reported. In these cases, reaction endothermicities were used to estimate lower limits for the reaction activation energies, E . The combination of an E lower limit with an estimated Arrhenius A factor upper limit, based on the largest A factor observed in OH + halocarbon reactions, was considered as providing a more realistic (and considerably lower) upper limit for the reaction rate coefficient.

The reactions of atmospheric trace species with O(¹D) proceed via several possible exothermic reaction pathways: (1) collisional (physical) quenching of O(¹D) to ground state oxygen atoms, O(³P), (2) abstraction or an insertion-elimination mechanism, and (3) reactive quenching to form O(³P) and products other than the reactant, including stable and radical species. Channels 2 and 3 lead to the loss of the reactant and contribute to determining the reactant's atmospheric lifetime. Overall, total rate coefficients for O(¹D)

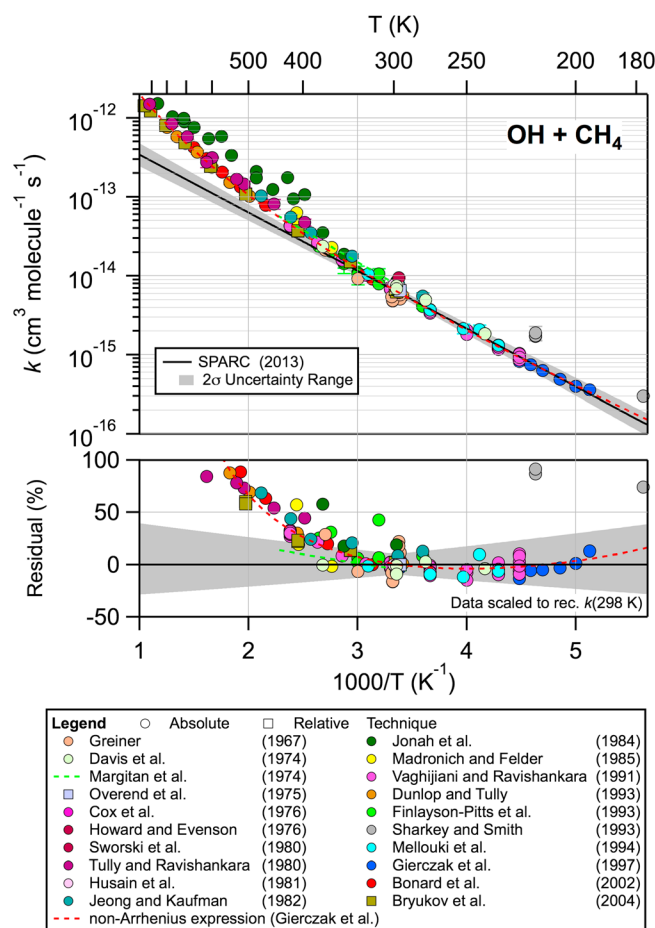


Figure 1. OH + CH₄ reaction data: (top) Compilation of experimental rate coefficient data from the literature and the recommended Arrhenius equation and uncertainty limits used in the present model calculations (see legend). The recommended Arrhenius equation parameters and uncertainty factors are given in Table 1. (bottom) Percent difference between reported rate coefficient data and recommended Arrhenius equation.

2.1. Rate Coefficient and Absorption Cross Section Uncertainty Estimates

The most stringent uncertainty limits (at the 2σ uncertainty level) justified by the available experimental data were reported in SPARC [2013]. The rate coefficient uncertainties followed the formalism given in JPL10-6

$$f(T) = f(298\text{ K}) \exp\left(\left|g\left(\frac{1}{T} - \frac{1}{298}\right)\right|\right) \quad (1)$$

where $f(T)$ is the uncertainty factor (1σ) for $k(T)$, $f(298\text{ K})$ is the estimated uncertainty factor for the room temperature rate coefficient, $k(298\text{ K})$, and g is a parameter used to describe the expected increase in uncertainty at temperatures other than 298 K. Upper and lower bounds of the rate coefficient are obtained by multiplying or dividing the recommended value, $k(T)$, by the factor $f(T)$. The 2σ uncertainty is given by $f(T)^2$. The estimated uncertainties are not statistical quantities but rather are based on an evaluation of the reliability of the experimental measurements and the level of agreement among different studies.

The UV absorption cross-section uncertainties are wavelength and temperature dependent with the regions of weaker absorption generally having greater uncertainty. In SPARC [2013], uncertainty estimates were provided

reactions, i.e., the loss of O(¹D), are typically highly efficient with O(¹D) loss occurring within 10 collisions or so. For halocarbons, the degree of collisional quenching increases with the degree of reactant fluorination. In general, O(¹D) reactions display only a weak, if any, temperature dependence. The available temperature dependent rate coefficient data for the O(¹D) + CH₄ and N₂O reactions shown in Figures 3 and 4 illustrate these points.

The VUV/UV absorption cross sections and their temperature dependences were addressed in greater detail in SPARC [2013] than in either of the NASA/JPL or IUPAC evaluations. Absorption cross section recommendations were obtained by comparing the level of agreement (spread) among multiple experimental data sets whenever possible. SPARC [2013] also included a detailed evaluation of hydrogen Lyman-α (121.567 nm) absorption cross sections, σ(L-α), and estimates of the cross section uncertainties were made. The σ(L-α) database is rather limited, and for some of the molecules included in the SPARC report, experimental values were not available. In those cases, values were estimated based on values reported for similar compounds or trends in cross section with the degree of fluorination.

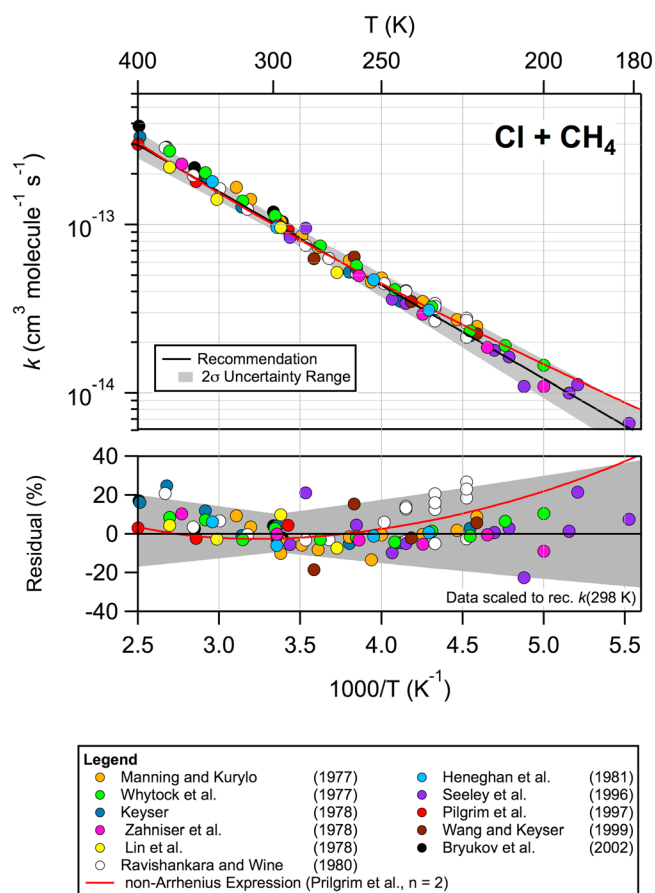


Figure 2. Cl + CH₄ reaction data: (top) Compilation of experimental rate coefficient data from the literature (see legend) used to derive the recommended rate coefficient temperature dependence given in SPARC [2013] and JPL10-6 and the recommended Arrhenius equation and uncertainty limits used in the present model calculations (see legend). The recommended Arrhenius equation parameters and uncertainty factors are given in Table 1. (bottom) Percent difference between reported rate coefficient data and recommended Arrhenius equation.

2.2. CH₄ Kinetic and Photochemical Data

There are numerous studies in the literature that have reported rate coefficient and product yield data for the OH, Cl, and O(¹D) reactions with CH₄



The rate coefficient recommendations given in SPARC, JPL10-6, and IUPAC are based on subsets of the available studies. Figures 1 and 2 show a compilation of kinetic data in an Arrhenius plot format, $\ln(k(T))$ versus $1/T$, for the OH and Cl reactions with CH₄ over the temperature range 190 to 500 K.

For the OH + CH₄ reaction, the majority of the experimental studies used absolute measurement techniques, and the rate coefficient recommendations are based primarily on studies performed after 1990; earlier studies were shown to have systematic errors in their rate coefficient determinations (see JPL10-6 and IUPAC reports for further details). The room temperature values used in the derivation of the 298 K rate coefficient recommendation agree to within ~15%. The studies of Vaghjiani and

for $\sigma(L-\alpha)$ and for the wavelength ranges of 169–190, 190–230, 230–286, and >286 nm. This was done to provide an error analysis that was sufficiently detailed to permit evaluation of the wavelength regions that are most critical to the molecule's photolytic loss. Cross-section uncertainties were parameterized using a formalism similar to that used for gas-phase reaction rate coefficients, where $p(298\text{ K})$ represents the 2σ (95% confidence) level uncertainty in the 298 K absorption cross-section data and w is a parameter used to represent an increase in the cross-section 2 uncertainty at other temperatures

$$p(T) = p(298\text{ K}) \exp\left(\left|w\left(\frac{1}{T} - \frac{1}{298}\right)\right|\right) \quad (2)$$

The recommended kinetic and photochemical parameters and associated estimated uncertainties for CH₄ and N₂O used in the present model calculations are given in Table 1. The kinetic and photochemical recommendations given in SPARC [2013] for the OH, Cl, and O(¹D) reactions with CH₄ and N₂O do not differ from those given in JPL10-6 except for the OH + CH₄ reaction which was the same as given in the IUPAC report. The estimated uncertainties in the kinetic and photo-chemical parameters, however, were revised for the OH + CH₄ reaction.

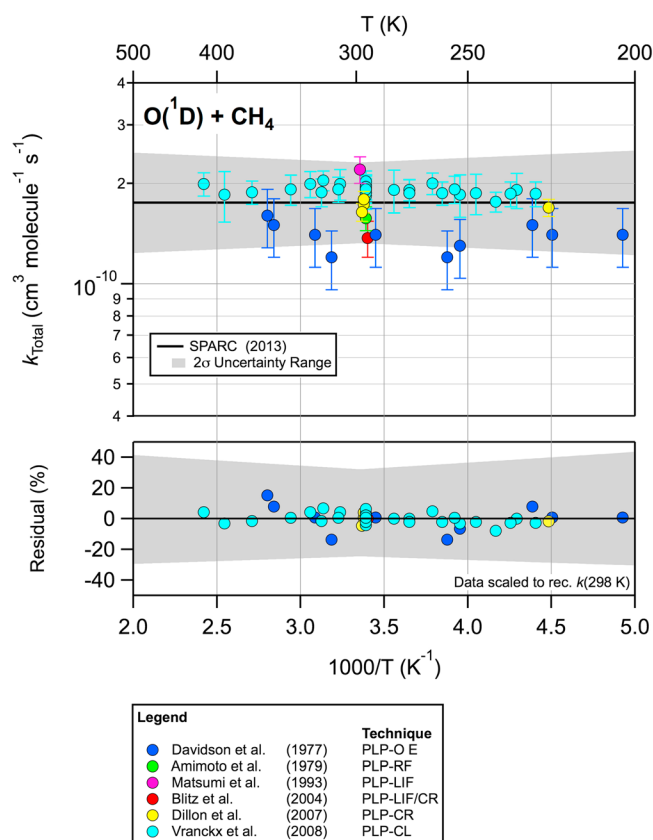


Figure 3. $\text{O}(^1\text{D}) + \text{CH}_4$ reaction data: (top) Compilation of experimental rate coefficient data from the literature and the recommended Arrhenius equation and uncertainty limits used in the present model calculations (see legend). The recommended Arrhenius equation parameters and uncertainty factors are given in Table 1. (bottom) Percent difference between reported rate coefficient data and recommended Arrhenius equation. Techniques include the following: PLP: pulsed laser photolysis, O E: $\text{O}(^1\text{D})$ emission, RF: resonance fluorescence, LIF: laser-induced fluorescence, CR: competitive reaction, CL: chemiluminescence.

for comparison with other experimental data and the recommended Arrhenius equations. Note that Pilgrim et al.'s study was conducted at temperatures greater than 292 K and an extrapolation of their reported $n = 2$ non-Arrhenius equation to lower temperature that extends well outside the range of their experimental data is displayed. The SPARC, JPL10-6, and IUPAC evaluations have reported simple Arrhenius equations to describe the rate of coefficient temperature dependence at temperatures less than 300 K, although non-Arrhenius equations are discussed within the JPL10-6 and IUPAC reports. Both equations reproduce the available experimental data to within the estimated range of uncertainty but differ systematically at low temperature. For example, the JPL10-6 Arrhenius fit to the $\text{Cl} + \text{CH}_4$ data is a factor of ~ 0.7 less than Pilgrim et al.'s non-Arrhenius equation at 200 K. Although Pilgrim et al.'s data set was not used in the derivation of the Arrhenius parameters for temperatures below 300 K, their non-Arrhenius equation can be used to check the atmospheric effects of possible Arrhenius curvature at low temperature, since their equation yields rate coefficient that lie near the upper bound of the currently recommended 95% confidence limits below 200 K (see Figure 2). The impact of using Pilgrim et al.'s non-Arrhenius rate coefficient expression ($n = 2$) versus the recommended Arrhenius equation for the $\text{Cl} + \text{CH}_4$ reaction on calculated atmospheric ozone is evaluated in the modeling section below. This illustrates the model sensitivity to a non-Arrhenius equation that falls within the JPL10-6 recommended uncertainty limits.

Ravishankara [1991] and Gierczak et al. [1997] were used to define the rate coefficient temperature dependence at low temperature (see Figure 1). The recommended uncertainties in the low-temperature region are greater than the reported uncertainties in the experimental data as a result of the limited data currently available.

There are a number of experimental studies in the literature that have reported rate coefficient data for the $\text{Cl} + \text{CH}_4$ reaction with studies covering the temperature range of 181 to 800 K. The agreement among the various studies is $\pm 15\%$ at 298 K, with a slightly greater spread in the experimental data at other temperatures as shown in Figure 2. The individual studies are too numerous to discuss here, and the reader is referred to JPL10-6 and IUPAC for more detail and explanation of what studies were used to establish the recommended rate coefficient. Several studies have proposed non-Arrhenius equations to better describe the OH and $\text{Cl} + \text{CH}_4$ reaction temperature dependence using a rate coefficient expression with the form $k(T) = A T^n \exp(-E/RT)$, where n is either fixed to a value of 2 or allowed to vary in a fit to the experimental data. The expressions provided in Gierczak et al.'s [1997] study of the $\text{OH} + \text{CH}_4$ reaction and Pilgrim et al.'s [1997] study for the $\text{Cl} + \text{CH}_4$ reaction are included in Figures 1 and 2

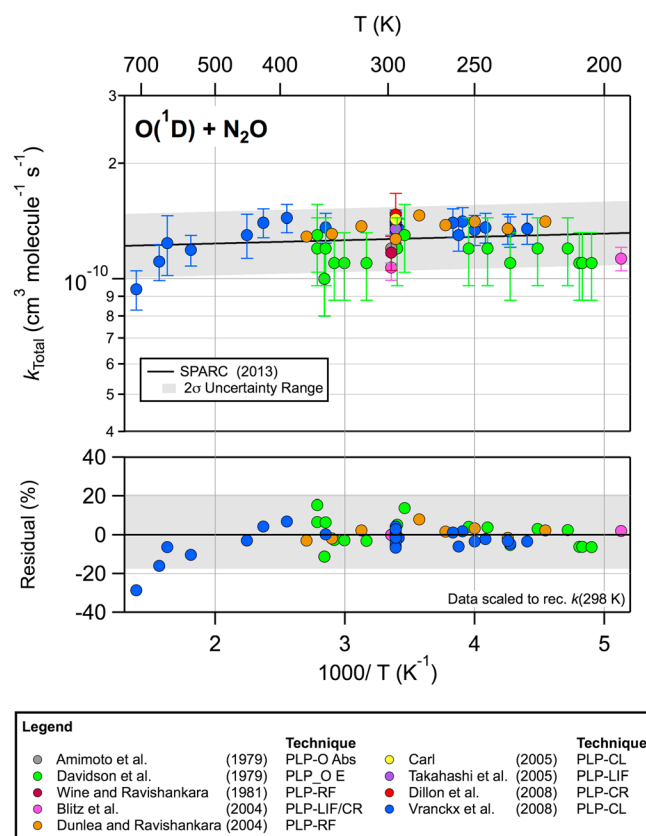


Figure 4. $O(^1D) + N_2O$ reaction data: (top) Compilation of experimental rate coefficient data from the literature and the recommended Arrhenius equation and uncertainty limits used in the present model calculations (see legend). The recommended Arrhenius equation parameters and uncertainty factors are given in Table 1. (bottom) Percent difference between reported rate coefficient data and recommended Arrhenius equation. Techniques include the following: PLP: pulsed-laser photolysis, O Abs, $O(^3P)$ absorption, O E: $O(^1D)$ emission, RF: resonance fluorescence, LIF: laser induced fluorescence, CR: competitive reaction, CL: chemiluminescence.

$\sigma(L-\alpha) = 1.85 \times 10^{-17} \text{ cm}^2 \text{ molecule}^{-1}$ with $p(298 \text{ K}) = 1.3$ and $w = 0$. These values are used in the present model calculations.

2.3. N_2O Kinetic and Photochemical Data

On the basis of reaction thermochemistry, SPARC reported rate coefficient recommendations for the OH and Cl reactions with N_2O to be extremely small (see Table 1), which results in these reactions being unimportant atmospheric loss processes for N_2O .

The total rate coefficient for the $O(^1D) + N_2O$ reaction



has been measured extensively with nine independent studies reported in the literature. A summary of the total rate coefficient results from these studies, i.e., $O(^1D)$ loss, is shown in Figure 4. The measurements cover the temperature range from 195 to 719 K and indicate a slight negative temperature dependence, $E/R = -20 \text{ K}$ (see Table 1 and Figure 4). The results from these studies were reviewed in JPL10-6, and no new studies have appeared since that report was finalized. The recommendation for the total rate coefficient at

There are five independent laboratory studies of the $O(^1D) + CH_4$ reaction reported in the literature that cover the temperature range of 198 to 413 K. The temperature-dependent studies observe no appreciable temperature dependence of the reaction rate coefficient over this temperature range. The recommended total rate coefficient given in Table 1 was based on the studies of Amimoto *et al.* [1979], Dillon *et al.* [2007], and Vranckx *et al.* [2008b], while the recommended uncertainty limits encompass the results from Davidson *et al.* [1977] and Blitz *et al.*'s [2004] studies (see Figure 3). In addition to reporting the total rate coefficient, Vranckx *et al.*'s [2008b] study established with high precision that the reactive yield for this reaction was near unity, $1.0 + 0/0.002$, over the temperature range of 227 to 413 K; i.e., there is very little $O(^1D)$ collisional quenching in this reaction.

The UV ($\lambda > 169 \text{ nm}$) absorption spectrum of CH_4 is sufficiently weak that photolysis in this wavelength region makes a negligible contribution to its atmospheric loss. The Lyman- α cross section of CH_4 has been extensively studied with direct measurements at 121.567 nm and in the surrounding wavelength region (see SPARC). The direct measurements and cross-section values obtained by interpolation to 121.567 nm agree to within $\sim 20\%$. SPARC recommended

Table 1. Kinetic and Photochemical Parameters and Uncertainties Used in GSFC 2-D Model Calculations Presented in This Work^a

Reaction	CH ₄		N ₂ O	
	$k(T)$ ^b	$f(298\text{ K})/g$	$k(T)$ ^b	$f(298\text{ K})/g$
Cl	$7.3 \times 10^{-12} \exp(-1280/T)$	1.05/50	$<1 \times 10^{-17}$	–
OH	$1.85 \times 10^{-12} \exp(-1690/T)$	1.05/50	$<5 \times 10^{-17}$	–
O(¹ D)				
Total reaction; O(¹ D) loss	$1.75 \times 10^{-10} \exp(-0/T)$	1.15/25	$1.19 \times 10^{-10} \exp(20/T)$	1.1/25
Reaction branching ratio	1	$^{+0}_{-0.002}$	0.39 (N ₂ + O ₂) 0.61 (2NO)	0.06 ^e
Photodissociation	Cross section ^c	$p(298\text{ K})/w$	Cross section ^c	$p(298\text{ K})/w$
Lyman- α	1.85×10^{-17}	1.3/–	2.4×10^{-17}	1.5/–
169–190 nm	–	–	d	1.12/60
190–230 nm	–	–	d	1.08/20
230–286 nm	–	–	d	1.12/–
>286 nm	–	–	d	1.3/–

^aThe $f(298\text{ K})$ and g are the 1σ (67% confidence level) values where the uncertainty at temperature T (K) is given by $f(T) = f(298\text{ K})\exp\{g(1/T - 1/298)\}$. The $p(298\text{ K})$ and w are the 2σ (95% confidence level) values where the uncertainty at temperature T (K) is given by $p(T) = p(298\text{ K})\exp\{w(1/T - 1/298)\}$.

^bReaction rate coefficients in $\text{cm}^3 \text{ molecule}^{-1} \text{ s}^{-1}$.

^cUnit: $\text{cm}^2 \text{ molecule}^{-1}$ (base e).

^dUV spectrum and temperature dependence taken from *Sander et al.* [2011].

^eAbsolute uncertainty in the 2NO channel.

298 K is a weighted average of the data from *Davidson et al.* [1979], *Amimoto et al.* [1979], *Wine and Ravishankara* [1982], *Blitz et al.* [2004], *Dunlea and Ravishankara* [2004], *Carl* [2005], *Takahashi et al.* [2005], *Dillon et al.* [2008], and *Vranckx et al.* [2008a]. The temperature dependence of the rate coefficient was derived from the results of Davidson et al., Dunlea and Ravishankara, and Vranckx et al. using only data at $<400\text{ K}$ after scaling to the recommended $k(298\text{ K})$ value. The recommended 2σ uncertainty range in the total rate coefficient is included in Figure 4. The reactive channels (4a + 4b) of the O(¹D) + N₂O reaction have a combined yield greater than 99% [*Vranckx et al.*, 2008a].

The branching ratio for the O(¹D) + N₂O reaction and its temperature dependence, which was not considered in SPARC, is an additional factor in evaluating the impact of this reaction on calculated stratospheric ozone; i.e., channel 4a leads to ozone destruction while channels 4b and 4c do not. The branching ratio for the reactive channels 4a and 4b has been measured experimentally only at room temperature, 298 K. *Cantrell et al.* [1994] measured the branching ratio, $k(\text{NO} + \text{NO})/k(\text{total})$ and combined their results with previous literature data and recommended a value of 0.61 ± 0.06 (2σ uncertainty), which was adopted in JPL10-6 and SPARC. Note that the rate coefficient uncertainties reported in JPL10-6, $f(298\text{ K}) = 1.1$ and $g = 25$, include the uncertainty in the reaction branching ratio. The sensitivity of calculated ozone to the branching ratio value is evaluated in the modeling section below.

Numerous studies have reported data for the UV absorption spectrum of N₂O (see SPARC and JPL10-6) that leads to its photodissociation



which occurs primarily in the stratosphere. The cross-section results of *Selwyn et al.* [1977] provide the basis of the SPARC and JPL10-6 recommendations for the wavelengths most critical to atmospheric photolysis. The spread in the experimental data from other studies is $\sim 10\%$, or less, near the peak of the spectrum at $\sim 182\text{ nm}$, while the spread in the available data is greater at longer wavelengths. The N₂O cross-section study by *Rontu Carlon et al.* [2010] performed at 183.95, 202.206, 206.200, and 213.857 nm over the temperature range of 210–350 K is in excellent agreement, to within 3%, with the recommendations. The p

(298 K) uncertainty factors given in Table 1 were reduced from those reported in JPL10-6 based primarily on the results from Rontu et al.'s study. Note that the JPL10-6 recommended uncertainty includes both the cross section and quantum yield uncertainties. It is, however, well established that the quantum yield for photodissociation of N₂O is essentially unity over the wavelength range critical to atmospheric photolysis, 195–230 nm, and the photoproducts are predominately N₂ and O(¹D) [Sander et al., 2011]; the N(⁴S) + NO(²Π) channel photolysis yield is less than 1% [Greenblatt and Ravishankara, 1990]. Nishida et al. [2004] reported the yield of O(³P) at 193 nm to be 0.005 ± 0.002. The recommended *w* uncertainty factors were based on a consideration of the agreement among the data of Selwyn et al. [1977], Mérienne et al. [1990], and Rontu et al. [2010].

There are no direct Lyman- α cross-section measurements for N₂O available in the literature. However, the VUV spectrum of N₂O in this general wavelength region has been reported in several studies (see SPARC). The Chan et al. [1994] and Hitchcock et al.'s [1980] studies agree to within 6% at 124 nm, while the value reported by Bertrand et al. [1975] at 123.6 nm is less by nearly a factor of 3. A linear interpolation of Chan et al.'s spectrum was used to derive a recommended Lyman- α cross section of 2.4×10^{-17} cm² molecule⁻¹. The interpolation assumes no significant structure in this region of the spectrum. Uncertainty factors of *p*(298 K) = 1.5 and *w* = 0 were assigned in SPARC based primarily on the lack of direct cross-section measurements at Lyman- α .

3. Model Simulations

The NASA/GSFC 2-D coupled chemistry-radiation-dynamics model was used to evaluate the impact of the CH₄ and N₂O kinetic and photochemical uncertainties on the calculated lifetimes and on the ozone abundance and trends. The GSFC 2-D model has been used in stratospheric ozone assessments [WMO 2007, 2011, 2014] and in studies pertaining to the chemistry-climate coupling of the middle atmosphere. The residual circulation framework used in 2-D models has been shown to provide realistic simulations of atmospheric transport on long time scales (>30 days). The model ozone, temperature, and long-lived tracer simulations are in good overall agreement with a variety of observations in reproducing transport-sensitive features in the meridional plane [Fleming et al., 2011]. The 2-D model accounts for CO₂ induced changes in surface temperature (including sea surface temperature), latent heating, and tropospheric water vapor by parameterizing these quantities using the CO₂ ground boundary condition and sensitivity factors derived from the Goddard Earth Observing System chemistry-climate model (GEOSCCM) simulations [Oman et al., 2010]. The resulting tropospheric and stratospheric temperature changes, acceleration of the stratospheric Brewer-Dobson circulation, and stratospheric ozone changes in the 2-D model compare well with the GEOSCCM for 1960–2100 [Fleming et al., 2011], illustrating that the 2-D model captures the basic processes responsible for long-term stratospheric changes. For the present study, the computational speed of the 2-D model allowed numerous long-term sensitivity simulations to be performed for 1960–2100 to evaluate the present-day and long-term ozone impacts due to the CH₄ and N₂O loss uncertainties. Although the GSFC 2-D model is free running, there is negligible year-to-year variability (unlike 3-D chemistry-climate Models (CCMs)). Therefore, in the results shown below, for present-day conditions, a single yearly average (e.g., 2000) is sufficient to isolate the changes due strictly to the loss rate uncertainties (i.e., it is not necessary to average over multiple years).

For part of this work, we also used the Global Modeling Initiative (GMI) three-dimensional (3-D) chemistry and transport model (CTM) [Duncan et al., 2007; Strahan et al., 2007]. The GMI model is driven by the NASA Modern Era Retrospective-Analysis for Research and Applications meteorological analyses for the time period of 1979 to present ([Rienecker et al., 2011] see also the website <http://gmao.gsfc.nasa.gov/research/merra/>). As will be shown, the Cl + CH₄ reaction has a moderate impact on ozone in the polar region for present-day levels of atmospheric chlorine loading. We used both the GMI and 2-D models to investigate the polar ozone response to the Cl + CH₄ uncertainty for present-day conditions.

Both the 2-D model and GMI simulations use surface boundary conditions from World Meteorological Organization [WMO, 2011] for the ODSs. For the long-lived GHGs, the Coupled Model Intercomparison Project Representative Concentration Pathway (RCP) medium scenario 4.5 ("historic" scenario before 2005) [Meinshausen et al., 2011] is used for the baseline, following the model simulations performed for the

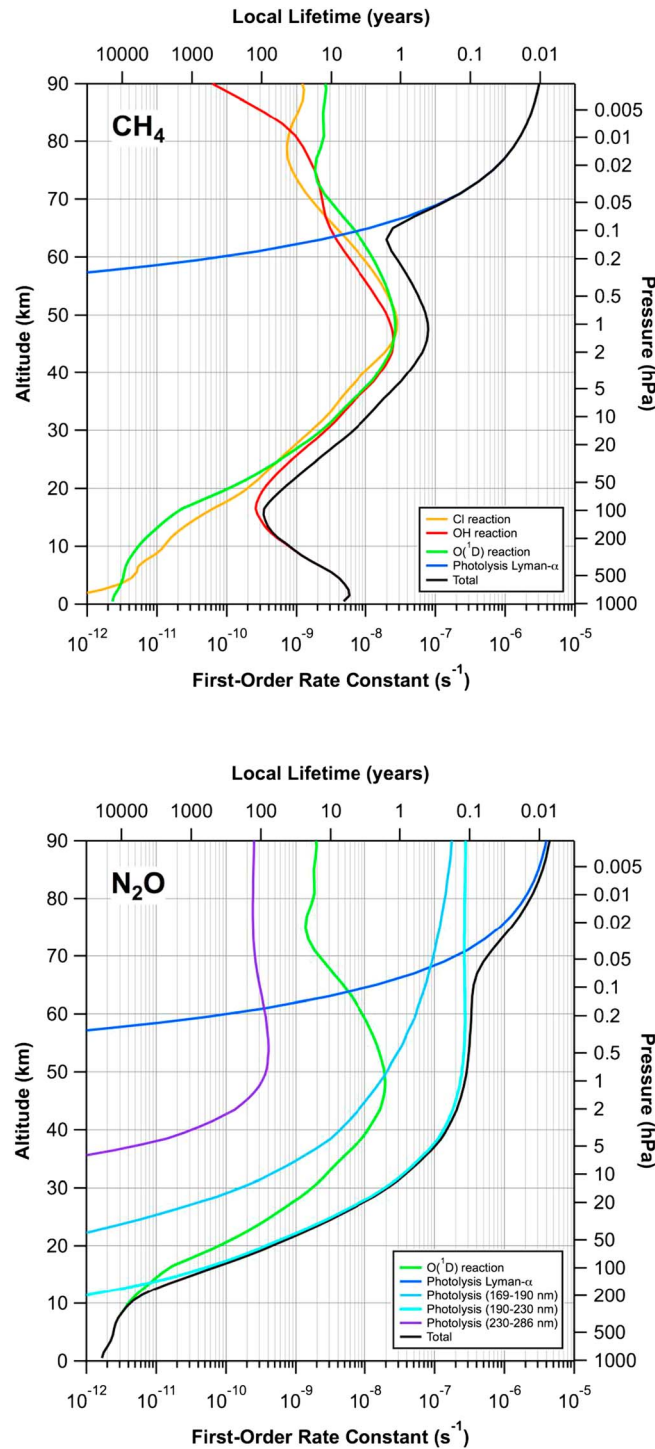


Figure 5. Global annual average local lifetimes for various gas-phase loss processes of (top) CH₄ and (bottom) N₂O calculated using the GSFC 2-D model for year 2000 steady state conditions.

tropospheric ozone response to the OH + CH₄ uncertainty is essentially the same using Spivakovsky et al.'s OH versus the model-computed (interactive) OH field, both for present-day conditions and projections into the future. We note that the stratospheric and mesospheric OH and atmospheric O(¹D) and Cl atom profiles are calculated in the 2-D model for all simulations presented in this study.

SPARC report. We also discuss 2-D model simulations illustrating the future impact of low and high GHG scenarios. Both the GMI and 2-D model simulations use constant solar flux and background stratospheric aerosol density conditions for all years.

The 2-D model was also used to investigate the long-term impact of uncertainty in the OH + CH₄ reaction. This reaction affects tropospheric ozone via the NO_x-induced ozone production cycle [e.g., Brasseur and Solomon, 2005]. To more properly simulate this mechanism, production and loss of tropospheric NO_y in the 2-D model are based on output from GMI for present-day conditions. These include surface NO_x emissions, NO_x production from lightning, and HNO₃ washout. The resulting 2-D model tropospheric ozone response to a steady state CH₄ perturbation (0.5 ppmv) was similar to that obtained in the GMI model, as was the ozone response to the OH + CH₄ reaction uncertainty. We note that because tropospheric NO_x is based on present-day conditions, the past or future CH₄ impact on ozone does not include the effect due to long-term changes in tropospheric NO_x.

In SPARC [2013], models that did not include detailed tropospheric chemistry (including the 2-D model used here) used a specified (noninteractive) monthly varying tropospheric OH field documented in Spivakovsky et al. [2000]. For the present study, we also specify tropospheric OH in the same manner. However, the model-computed OH differs from Spivakovsky et al. mainly in the lower troposphere, where the model has larger concentrations. The OH fields are similar in the middle and upper troposphere and are within ±10% in the tropics where most of the OH induced loss occurs. Sensitivity tests showed that the middle-upper

Table 2. Global Annually Averaged Fractional Loss Contributions Calculated From the 2-D Model for 2000 Steady State Conditions With Input Kinetic and Photochemical Parameters From SPARC [2013] (Table 1)^a

Compound	$h\nu$ (121.567 nm)	$h\nu$ (169–190 nm)	$h\nu$ (190–230 nm)	$h\nu$ (230–286 nm)	$h\nu$ (>286 nm)	$h\nu$ Total	O(¹ D) Reactive Loss	OH Reaction	Cl Reaction
N ₂ O	<0.001	0.012	0.888	<0.001	–	0.901	0.099	–	–
CH ₄	<0.001	–	–	–	–	<0.001	0.019	0.966	0.015

^aUsing input parameters from JPL10-6 [Sander *et al.*, 2011] gives identical fractional loss contributions.

3.1. N₂O and CH₄ Lifetimes and Uncertainties

We first present 2-D model calculations of the local lifetimes for the individual N₂O and CH₄ loss processes, the total global lifetime, and the associated uncertainty ranges (see SPARC for details). Figure 5 shows vertical profiles of the global annually averaged local lifetimes for 2000 steady state conditions using the kinetic and photochemical recommendations listed in Table 1. Figure 5 includes all of the loss processes, although as shown, not all make a significant contribution to the total local lifetime. To identify the wavelength regions of greatest importance in photolysis, the photolytic loss was divided into Lyman- α and the wavelength ranges of 169–190, 190–230, 230–286, and >286 nm. The fractional contributions of each loss process to the total vertically integrated global loss are listed in Table 2 for the recommendations listed in Table 1. These are identical to the fractional contributions obtained when using the recommendations from JPL10-6 [Sander *et al.*, 2011]. The fractional contribution breakdown identifies the most critical loss processes for each molecule as well as potential focus areas for future laboratory studies. For N₂O, photolysis in the 190–230 nm wavelength region is the dominant loss process, with the O(¹D) reaction making a minor contribution. For CH₄, atmospheric loss in the troposphere is dominated by its reaction with the OH radical; in the stratosphere, reactions with OH, O(¹D), and the Cl atom make roughly similar contributions (Figure 5). In the mesosphere above 65–70 km, the losses for both molecules are dominated by Lyman- α photolysis.

We also evaluated the uncertainty (range) in calculated atmospheric loss and lifetimes due to the uncertainties in the input kinetic and photolytic parameters. To do this, model simulations were made with the input parameters set to their 2 σ uncertainty lowest values (slow) and to their 2 σ uncertainty greatest values (fast) and compared with the baseline calculations presented in Figure 5. Figure 6 shows the uncertainty in the local loss rates for N₂O and CH₄ and a breakdown of the contribution from the different loss processes (for 2000 steady state conditions). For CH₄, the total uncertainty in the troposphere is in the range of ± 10 –40% due almost exclusively to the uncertainty in the OH + CH₄ reaction rate coefficient. The increase in the uncertainty with increasing altitude throughout the troposphere and lower stratosphere is due to the increased uncertainty in the rate coefficient at lower temperatures. In the stratosphere, the total local loss uncertainty is $\sim \pm 30$ % due to roughly equal contributions from the O(¹D), OH, and Cl reactions. For N₂O, the uncertainty in the stratospheric loss is in the range of ± 10 –20% due mainly to photolysis in the wavelength range of 190–230 nm.

The ranges in the total global lifetimes of N₂O and CH₄ computed from the fast (minimum lifetime) and slow (maximum lifetime) uncertainty limits are listed in Table 3, using input kinetic and photochemical parameters from Table 1 [SPARC, 2013] and JPL10-6 [Sander *et al.*, 2011]. These lifetimes are computed as the ratio of the total global atmospheric burden to the vertically integrated annually averaged global total loss rate, following the methodology used in SPARC. While the baseline lifetimes change very little between JPL10-6 and the current recommendations, the 2 σ uncertainty range is significantly reduced for the current recommendations compared with JPL10-6: ± 6 % versus ± 11 % for N₂O and ± 13 % versus ± 25 % for CH₄. Table 3 also gives the lifetimes separated by loss in the troposphere (surface to the tropopause, seasonally and latitude dependent), stratosphere, and mesosphere (<1 hPa). The lifetimes (τ) are computed using the global atmospheric burden and the loss rate integrated over the different atmospheric regions such that

$$\frac{1}{\tau_{\text{Tot}}} = \frac{1}{\tau_{\text{Trop}}} + \frac{1}{\tau_{\text{Strat}}} + \frac{1}{\tau_{\text{Meso}}}$$

The short tropospheric lifetime for CH₄ reflects the dominant OH reactive loss; the CH₄ stratospheric lifetime is ~ 160 years. For N₂O, the vast majority of the loss occurs in the stratosphere via photolysis and reaction with O(¹D) so that the stratospheric lifetimes are similar to the total global values. In the mesosphere, short-

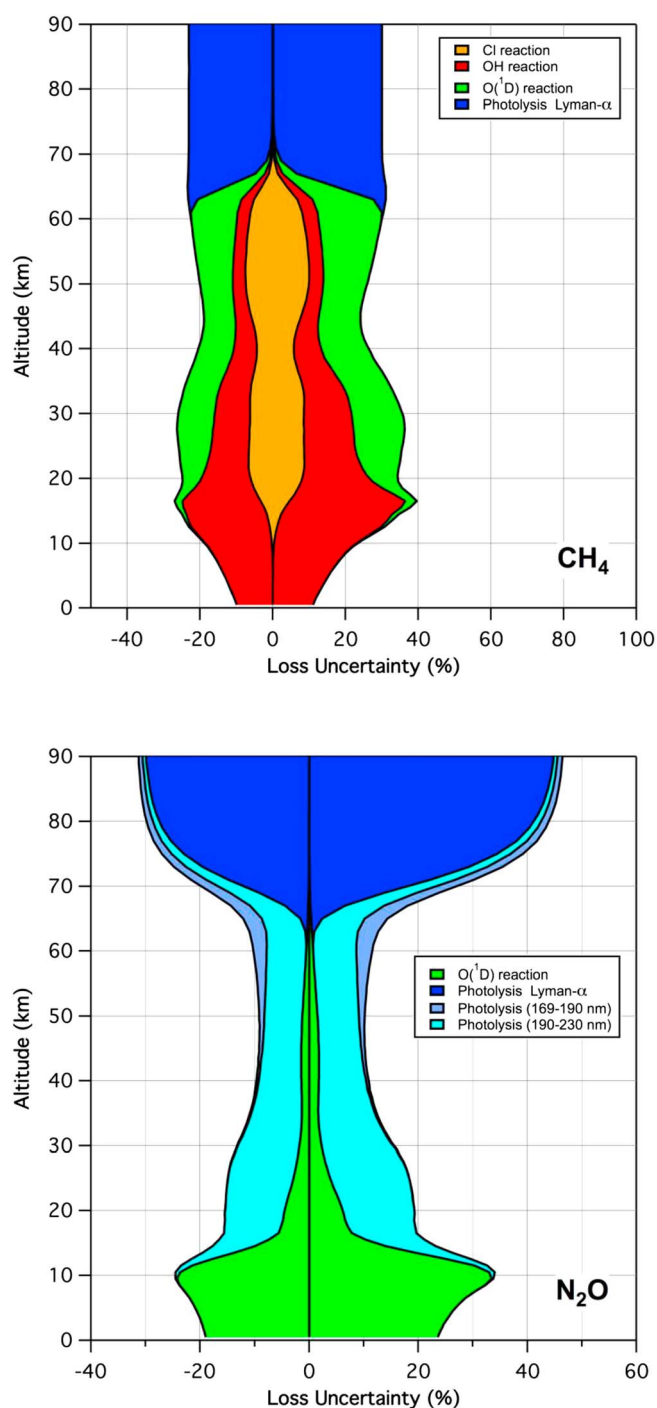


Figure 6. Uncertainty in the global annual average local loss rate calculated from the GSFC 2-D model using SPARC [2013] recommended kinetic and photochemical parameters and 2σ uncertainties for (top) CH₄ and (bottom) N₂O (see Table 1). The simulations are for the year 2000 steady state conditions.

(Figure 7, middle row) maximizes in the upper troposphere and very low stratosphere, with ozone decreases (increases) of 3–4% mainly due to the reduction (enhancement) of the NO_x-induced ozone production cycle following methane oxidation [e.g., Brasseur and Solomon, 2005]. The OH + CH₄ uncertainty also has a secondary and opposite response in the upper stratosphere, with an ~0.5% ozone increase

wavelength UV and Lyman- α photolysis are important local loss processes for both molecules (Figure 5). However, the global mesospheric lifetimes are quite long (>4000 years) since the density weighted loss rates are very small for the mesosphere.

We note that the baseline lifetimes presented in Table 3 do not supersede those recommended in SPARC. Rather, they serve as a reference point to illustrate (1) the changes in lifetimes between JPL10-6 and SPARC, (2) the range of lifetimes obtained using the uncertainty limits on the various loss processes, and (3) the distribution of lifetimes among the different atmospheric regions, all of which are computed from one individual model.

3.2. Impact of Uncertainties on Ozone

3.2.1. CH₄ Loss Processes

The 2σ uncertainties in the model input kinetic and photolytic parameters of CH₄ and N₂O affect not only the loss rates and lifetimes of these molecules but also substantially impact calculated atmospheric ozone. Figure 7 shows the year 2000 annual average ozone change (%) computed with the individual CH₄ loss parameters from Table 1 set to their 2σ uncertainty lowest values (slow; Figure 7, left) and to their 2σ uncertainty greatest values (fast; Figure 7, right), relative to the baseline simulation. Here the ozone changes using the slow rates are roughly similar in magnitude and opposite those using the fast rates. The ozone changes in the mesosphere above 60 km are generally small, <1%, and are not shown.

In the upper stratosphere, the slow (fast) O(¹D) loss yields ozone increases (decreases) of 1% mainly due to the reduction (enhancement) of the odd hydrogen (HO_x) ozone loss cycles. The effect of the slow (fast) OH loss

Table 3. Global Annually Averaged Atmospheric Lifetimes (Years) Calculated From the 2-D Model for 2000 Steady State Conditions With the Recommended Input Kinetic and Photochemical Parameters and the Estimated 2σ Uncertainty Limits From SPARC [2013] and JPL10-6 [Sander et al., 2011] as Given in Table 1

Compound	Model Input	Lifetime (Total)	Lifetime Range ^a	% Range in Lifetime	Tropospheric	Stratospheric	Mesospheric
N ₂ O	SPARC	125.2	118.1–132.3	±5.7	10990	127.5	19250
	JPL10-6	125.2	113.0–139.6	±11	11010	127.5	19360
CH ₄	SPARC	9.32	8.17–10.6	±13	9.92	159.6	4223
	JPL10-6	9.56	7.43–12.2	±25	10.2	163.3	4168

^aLifetime limits calculated using the 2σ uncertainty limits of the model input parameters.

(decrease) due to the reduction (enhancement) of the odd hydrogen (HO_x) ozone loss cycles. These responses are similar to the GMI simulations (within 10% in magnitude, not shown). Uncertainty in the Cl + CH₄ → CH₃ + HCl reaction (Figure 7, bottom row) affects the conversion of active to reservoir chlorine species throughout the stratosphere and has a moderate impact in the southern hemisphere (SH) polar lower

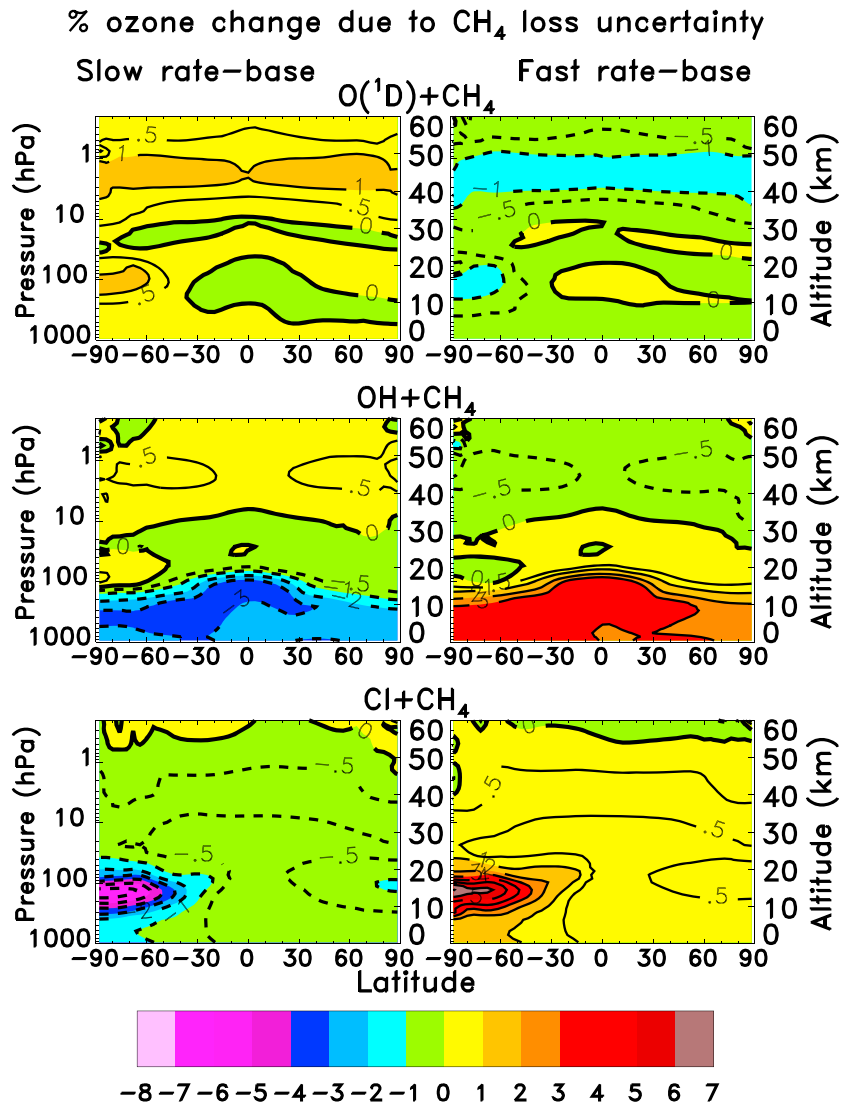


Figure 7. Percentage change in annual average ozone for year 2000 due to the (left) 2σ slow and (right) 2σ fast uncertainties (see text) in the CH₄ loss processes indicated. Changes are taken relative to the baseline. The contour intervals are ±1% and include the ±0.5% contours.

Total ozone change (DU) due to Cl+CH₄ uncertainty

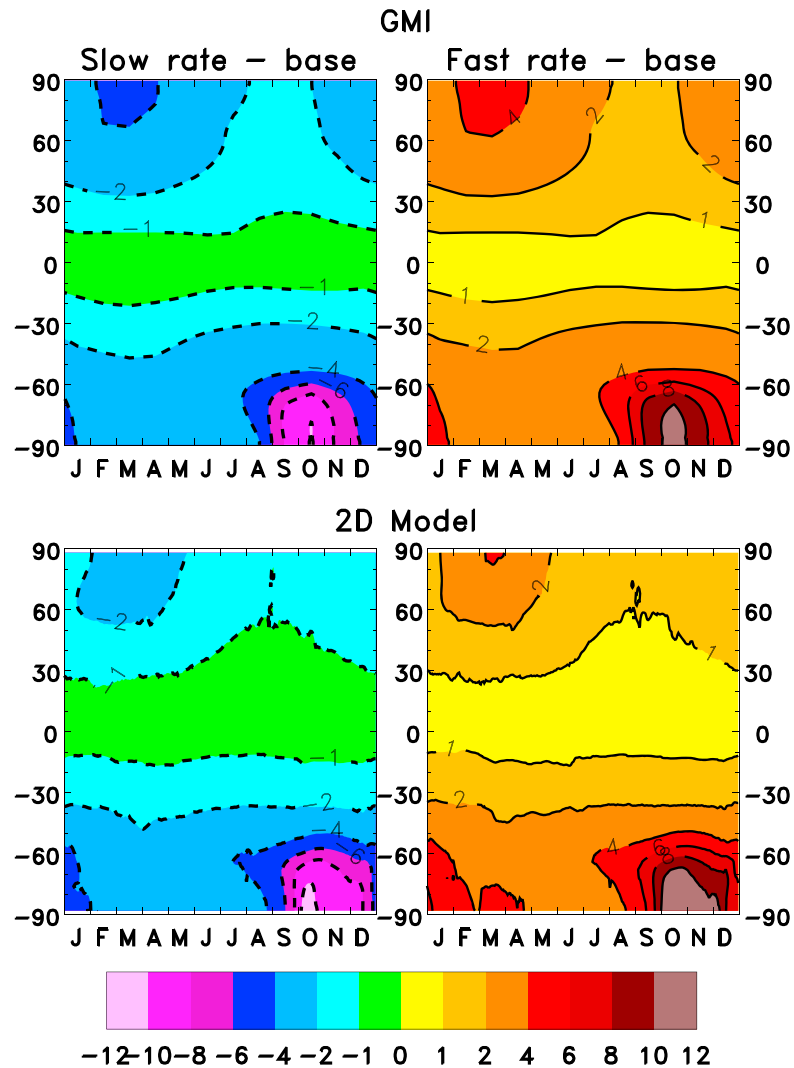


Figure 8. Seasonal change in total column ozone due to the (left column) 2σ slow and (right column) 2σ fast uncertainty in the Cl + CH₄ reaction. Shown are results from the GMI (top row) 3-D CTM and the (bottom row) 2-D model averaged over 2009–2013. Changes are taken relative to the baseline. See text for details. The contour intervals are ±2 DU and include the ±1 DU contours.

stratosphere/upper troposphere. Here the slow (fast) uncertainty yields ozone decreases (increases) of 6–7%. The Cl + CH₄ uncertainty gives secondary maxima responses of the same sign in the northern hemisphere (NH) polar lower stratosphere and the global upper stratosphere, with changes of slightly less than ±1% in both regions. The seasonal variations in these lower polar stratospheric responses are explored in more detail below. The O(¹D) + CH₄ reaction uncertainty also causes an ~±1% ozone change in the SH polar lower stratosphere (Figure 7, top row). Here a slower reaction allows more CH₄ to be available to react with Cl atoms, thereby enhancing the impact of the Cl + CH₄ reaction and leading to more ozone (with the opposite occurrence for the fast O(¹D) loss reaction). There is some indication that this process also occurs with the OH + CH₄ uncertainty (Figure 7, middle row), although this effect is masked by interference with the NO_x-induced ozone production cycle changes discussed above. Given the importance of the Cl + CH₄ reaction in the polar region, we note that the 2-D model uses longitudinal temperature probability distributions obtained from meteorological analyses to compute the polar stratospheric cloud formation and heterogeneous and gas phase reaction rates [Fleming *et al.*, 2011]. This helps account for the large zonal

asymmetries characteristic of the polar region during winter and spring. These probability distributions (based on climatologically averaged meteorological data and repeated each year) are superimposed on the model-computed zonal mean temperatures.

As a check of the fidelity of the 2-D model in simulating the Cl + CH₄ impact, we computed the ozone response to this reaction uncertainty using the GMI 3-D CTM. The year-to-year variations in the GMI response are generally small in the SH polar region, and the resulting ozone profile changes are generally similar to the 2-D model responses shown in Figure 7 (bottom). Total column ozone changes in the two models are also similar (Figure 8), illustrating that the 2-D model resolves the basic polar ozone response to this Cl + CH₄ perturbation (the changes in Figure 8 are averaged over 2009–2013 to account for the small year-to-year variations in the GMI model). The seasonal changes in Figure 8 maximize during the polar late winter-spring in both models, with changes of ±8–12 DU in the SH and ±2–4 DU in the NH. While this SH response is somewhat substantial (~±5–7% out of a background of ~170 DU), the NH response shown in Figure 8 is rather small, especially relative to the large interannual variability inherent in the NH polar late winter-spring. This hemispheric asymmetry in the sensitivity of the Cl + CH₄ reaction is likely due to two factors. In the SH, there is more conversion of chlorine reservoir species (HCl and ClONO₂) to radical forms via heterogeneous reactions on the surfaces of polar stratospheric cloud particles [e.g., WMO, 2011]. Also, the low ozone in the SH polar spring substantially elevates the Cl/ClO ratio, which significantly enhances the impact of the Cl + CH₄ reaction, compared with the NH [Douglass *et al.*, 1995]. We note also that the ozone sensitivity to the Cl + CH₄ uncertainty in the SH polar region is somewhat mitigated by the reaction ClO + CH₃O₂ → ClOO + CH₃O together with the heterogeneous reaction HCl + HOCl → Cl₂ + H₂O, which allow chlorine activation and ozone loss to continue in the presence of the reaction Cl + CH₄ [Crutzen *et al.*, 1992].

As described above and shown in Figure 2, the rate coefficient data available for the Cl + CH₄ reaction at the low temperatures representative of the polar regions show considerable spread. Both JPL10-6 and SPARC noted non-Arrhenius behavior for this reaction. However, due to the limited amount of data in the low-temperature region, they recommend an Arrhenius equation (Table 1) for use at temperatures below 300 K. If, in fact, non-Arrhenius behavior persists, this approach could lead to a systematic underestimate of the rate coefficient at the lower temperatures of interest compared to that obtained using a non-Arrhenius equation. The non-Arrhenius equation, as proposed by Pilgrim *et al.* [1997],

$$k(T) = 8.9 \times 10^{-13} \times (T/298)^2 \times \exp(-660/T) \quad (3)$$

falls within the upper range of the JPL10-6 recommended uncertainty limits and was used in the current model calculations to evaluate the significance of using a non-Arrhenius equation. Note that this is only a test case and does not imply that Pilgrim *et al.*'s equation is actually an accurate representation of the reaction rate coefficient at low temperatures. This non-Arrhenius equation is included in Figure 2 (red line) and when compared to the JPL10-6 and SPARC recommendations yields greater rate coefficient values at temperatures lower than ~265 K. A greater Cl + CH₄ rate coefficient converts more active to reservoir chlorine, which results in more ozone throughout most of the atmosphere (i.e., less ozone loss). Using this rate coefficient yields modest ozone increases in both the GMI and 2-D models as shown in Figure 9 for present-day conditions (2009–2013 average). For annually averaged profile ozone (Figure 9, top row), the maximum increase is +3–4% in the SH polar lower stratosphere/upper troposphere, with a secondary maximum of +0.5% in the NH polar lower stratosphere/upper troposphere. The impact in the upper stratosphere is minimal in both models (<+0.2%). The seasonal total column ozone increase (Figure 9, bottom row) again maximizes in late winter/early spring in each polar region: +7–8 DU in the SH and ~+2 DU in the NH. The response in the SH polar spring represents a 4–5% reduction in the depth of the ozone hole (7–8 DU increase out of ~170 DU).

Based, in part, on the good agreement between the 2-D and GMI models, the computational speed of the 2-D model was used to examine the long-term effects of the Cl and O(¹D) + CH₄ loss uncertainties (2σ) on October monthly mean total ozone in the southern polar region. Figure 10 (top) shows the 1960–2100 time series of the uncertainty simulations, expressed as the difference (in DU) from the baseline, where the slow (fast) uncertainties are depicted by the light (bold) lines. For the Cl loss reaction (orange lines), the slow (fast) uncertainty yields total column ozone decreases (increases) relative to the baseline. As discussed above

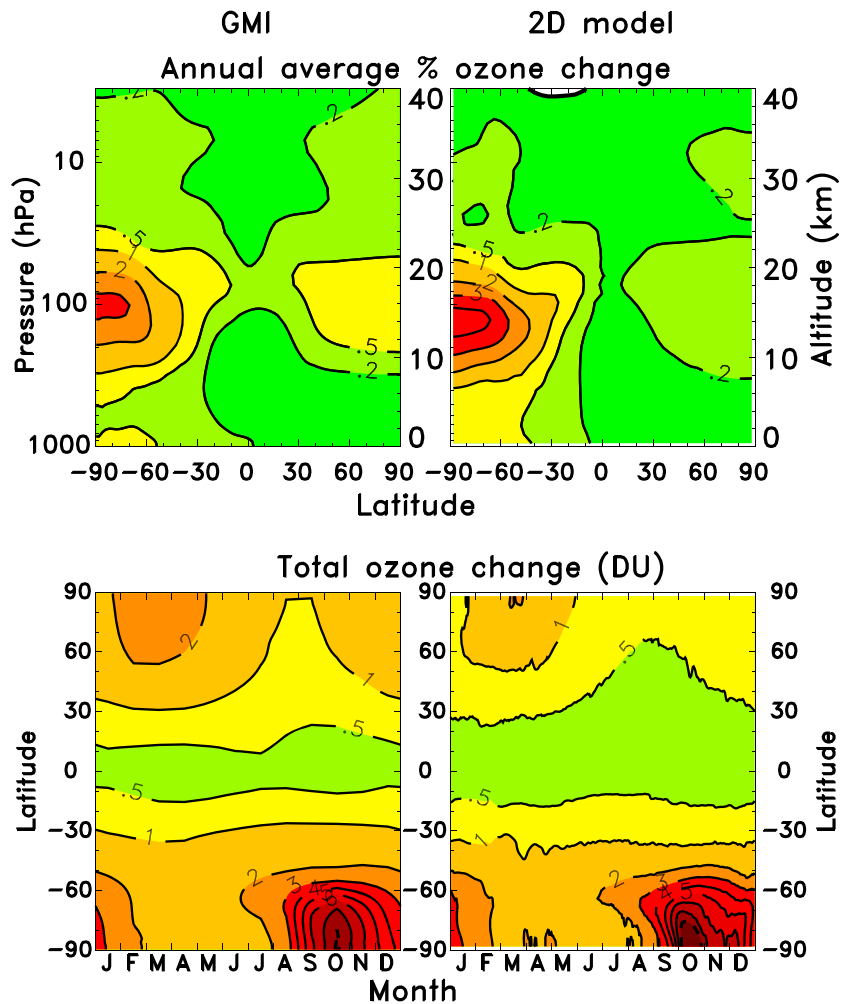


Figure 9. Change in present-day ozone using the Cl + CH₄ reaction non-Arrhenius rate coefficient expression given in equation (3) from *Pilgrim et al.* [1997] versus the Arrhenius equation recommendations given in JPL10-6 and SPARC (see Table 1). This non-Arrhenius equation should be considered an upper limit of possible non-Arrhenius behavior that falls within the JPL10-6 uncertainty range. Results from the GMI (left column) 3-D CTM and the (right column) 2-D model averaged over 2009–2013 are shown. (top row) The percentage change in annual average profile ozone; the contour intervals are +0, +0.5, +1, +2, +3, and +4. (bottom row) The seasonal change in total column ozone; the contour intervals are +1 DU and include the +0.5 DU contour.

(shown in Figure 7), the O(¹D) loss uncertainty (green lines) has a smaller but opposite effect, as a slower reaction allows more CH₄ to be available to react with Cl atoms, thereby enhancing the impact of the Cl + CH₄ reaction and leading to more ozone (with the opposite occurrence for the fast O(¹D) loss reaction). These ranges follow atmospheric chlorine loading: very small in 1960 (~±1 DU), increasing rapidly to a maximum in the late 1990s (±10–11 DU, ~±6%, for the Cl loss) and gradually diminishing through the 21st century. The polar total ozone response to the OH loss uncertainty is relatively small (<±1 DU) and is not shown in Figure 10.

The strong time dependence in the uncertainty ranges impacts the rate of ozone decline and recovery during 1960–2100. This is shown in Figure 10 (bottom), presented as the difference from 1960 values to emphasize the time dependence. We note that the time evolution of the baseline (black line) throughout the time period is very similar to the multimodel mean of several 3-D chemistry-climate models shown to have realistic transport as discussed in *Strahan et al.* [2011]. For reference, we also show ground-based ozone observations illustrating the range of observed interannual variability (symbols, updated from *Fioletov et al.* [2002]). The orange shading depicts the 2σ uncertainty range of the Cl loss uncertainty from Figure 10 (top) added to the baseline and illustrates the impact of the Cl + CH₄ uncertainty in the context of the overall

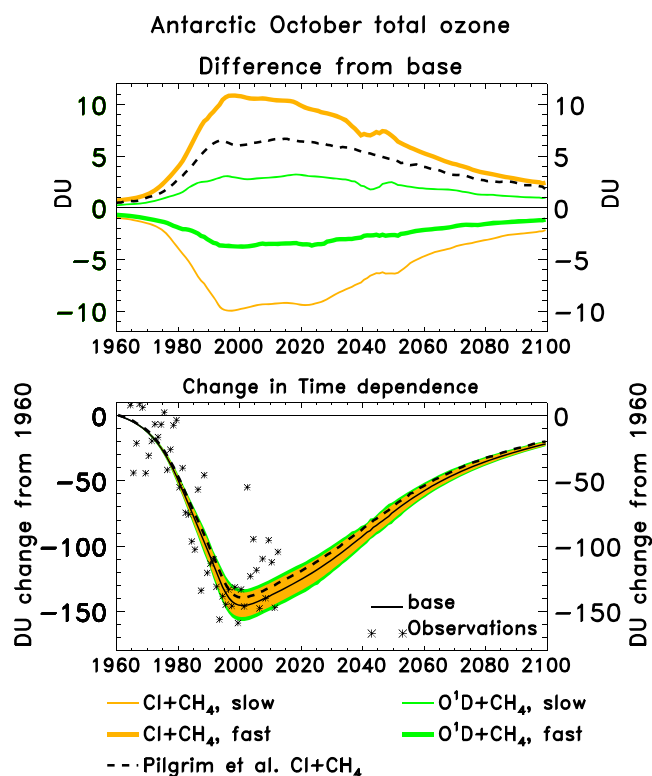


Figure 10. Time series of responses in October monthly mean total column ozone averaged over 60°S – 90°S due to uncertainties in the CH_4 loss reactions. (top) The 2σ uncertainty simulations for the Cl and $\text{O}(^1\text{D})$ loss reactions for CH_4 plotted as the difference from the baseline. The slow (fast) uncertainties are depicted by the light (bold) lines. A simulation using the Cl + CH_4 non-Arrhenius rate coefficient expression given in expression (3) from Pilgrim *et al.* [1997] (black dashed line) is also shown. (bottom) The changes in the time dependence: the range due to uncertainty in the Cl loss reaction from Figure 10 (top) added to the baseline (orange shading) and the range due to the combined uncertainty in the Cl and $\text{O}(^1\text{D})$ loss reactions from Figure 10 (top) added to the baseline (i.e., the slow (fast) Cl and fast (slow) $\text{O}(^1\text{D})$ loss responses have been combined, green shading). All simulations have been offset to be zero in 1960 to emphasize the time dependence. See text for details. The impact of the OH loss reaction is quite small and is not shown. The baseline simulation (black solid line), a simulation using Pilgrim *et al.*'s [1997] rate coefficient (equation (3), black dashed line), and ground-based observations updated from Fioletov *et al.* [2002] (symbols) are also shown.

± 3.4 DU), due to the very large future methane increase in RCP8.5 [Meinshausen *et al.*, 2011]. However, this effect is small compared to the long-term baseline ozone changes driven by chlorine loading (Figure 10).

Figure 10 also shows the long-term effect of using the non-Arrhenius equation (3) from Pilgrim *et al.* [1997] for the Cl + CH_4 reaction (black dashed line). This result is qualitatively similar to the 2σ fast uncertainty case for Cl + CH_4 , with more total ozone throughout 1960–2100 relative to the baseline, and a maximum change of +6–7 DU during the late 1990s to early 2000s (Figure 10, top). As was shown in Figure 9, this indicates that accounting for possible non-Arrhenius behavior of the Cl + CH_4 reaction at the lower temperatures characteristic of the SH polar stratosphere results in a small reduction in the depth of the ozone hole (compared to the baseline) for present-day levels of chlorine loading (Figure 10, bottom). Using a non-Arrhenius equation may provide a more realistic representation of the Cl + CH_4 rate coefficient, but further, research is needed to better define the rate coefficient parameterization at temperatures relevant for stratospheric modeling and to reduce its overall uncertainty, thereby reducing the range of ozone responses.

ozone changes during 1960–2100. This uncertainty range represents a small modification of the rate of change in the long-term ozone decline and recovery. The slow uncertainty limit leads to a faster ozone decline during 1960–2000, a deeper ozone hole, and a faster recovery through the 21st century; the fast uncertainty limit leads to a slower ozone decline, shallower ozone hole, and slower future recovery. Combining the impacts of the Cl and $\text{O}(^1\text{D})$ loss uncertainties added to the baseline yields a slightly larger range (green shading). Here the slow $\text{O}(^1\text{D})$ and fast Cl uncertainty limit simulations are added together to get the extreme positive ozone change, with the fast $\text{O}(^1\text{D})$ and slow Cl simulations added to get the extreme negative ozone change. These represent the absolute upper and lower limit impacts of the combined uncertainties. In 2000, this combined uncertainty range represents a modest impact on the depth of the ozone hole: ± 13 – 14 DU, i.e., $\sim \pm 9\%$ out of a baseline decline of 150 DU from 1960–2000. These CH_4 loss uncertainty impacts become increasingly less important through the 21st century as atmospheric chlorine loading decreases and are quite small by 2100.

There is a weak sensitivity of these responses to future CH_4 scenarios (see Table 4 which corresponds to Figure 10 (top) for RCP4.5). In 2100, the combined range of the $\text{O}(^1\text{D})$ and Cl uncertainty impacts is slightly larger for the RCP8.5 (high) scenario compared to RCP4.5 (± 5.5 versus

Table 4. Percentage Range in the Global Annually Averaged Total Column Ozone Change for Year 2100 due to the 2σ Uncertainties in the N_2O and CH_4 Loss Processes Indicated^a

Loss Process	RCP2.5 $\pm\%$ ($\pm\text{DU}$)	RCP4.5 $\pm\%$ ($\pm\text{DU}$)	RCP8.5 $\pm\%$ ($\pm\text{DU}$)
$J[\text{N}_2\text{O}]$	0.49 (1.4)	0.49 (1.4)	0.44 (1.3)
$\text{O}(^1\text{D}) + \text{N}_2\text{O}$ total reaction	2.3 (6.7)	2.3 (6.9)	2.0 (6.2)
$\text{O}(^1\text{D}) + \text{N}_2\text{O}$ branching ratio	0.98 (2.8)	0.99 (2.9)	0.85 (2.6)
$\text{O}(^1\text{D}) + \text{CH}_4$	0.04 (0.11)	0.05 (0.15)	0.08 (0.23)
$\text{OH} + \text{CH}_4$	0.37 (1.1)	0.43 (1.3)	0.75 (2.3)
$\text{Cl} + \text{CH}_4$	0.14 (0.41)	0.16 (0.46)	0.16 (0.49)
$\text{O}(^1\text{D}) + \text{CH}_4$ (Oct 60°S–90°S avg)	0.28 (0.96)	0.30 (1.1)	0.55 (2.0)
$\text{OH} + \text{CH}_4$ (Oct 60°S–90°S avg)	0.16 (0.57)	0.2 (0.7)	0.32 (1.2)
$\text{Cl} + \text{CH}_4$ (Oct 60°S–90°S avg)	0.55 (1.9)	0.65 (2.3)	0.94 (3.5)

^aResults using the RCP2.5 (low), RCP4.5 (medium), and RCP8.5 (high) greenhouse gas scenarios, with the ranges taken relative to the baseline for each scenario, are shown. The ranges in Dobson units are given in parentheses. The last three rows show the ranges in October 60°S–90°S average total ozone due to the CH_4 loss uncertainties. Results for RCP4.5 correspond to Figures 10, 11, and 14 (top graphs). Values were calculated from time-dependent 2-D model simulations.

For annually averaged global total ozone, the long-term impacts due to the 2σ uncertainties for all three CH_4 loss processes are shown in Figure 11. Figure 11 (top) shows the difference of the uncertainty simulations from the baseline using the RCP4.5 scenario and includes the impact of the OH loss uncertainty using RCP8.5 (red dash-dotted lines). The slow (fast) uncertainties are depicted by the light (bold) lines. As seen in Figure 7, slower (faster) rates of the Cl and OH loss reactions yield less (more) total ozone, with the opposite occurrence for the $\text{O}(^1\text{D}) + \text{CH}_4$ reaction. We note that although these simulations specify tropospheric OH from the present-day climatology of *Spivakovsky et al.* [2000], very similar total ozone responses were obtained when using the model computed tropospheric OH that interacts with changes in the background climate and chemistry (e.g., stratospheric ozone, tropospheric water vapor, and methane loading). Future tropospheric OH concentrations depend strongly on methane and are significantly different among the RCPs [e.g., *Voulgarakis et al.*, 2013; *Morgenstern et al.*, 2013], and we also obtained a strong OH and ozone dependence on the RCPs in the baseline simulations in Figure 11. However, the model computed tropospheric OH responses to the $\text{OH} + \text{CH}_4$ uncertainty perturbations performed here were very similar among the RCPs. The time-dependent ozone impacts of the $\text{OH} + \text{CH}_4$ reaction in Figure 11 primarily follow the CH_4 loading of the RCP scenarios (there is also a smaller effect due to long-term changes in the model stratospheric OH caused by CH_4 and climate-induced changes in stratospheric H_2O and long-term ozone-induced changes in $\text{O}(^1\text{D})$). For RCP4.5, the global total ozone impact of the OH loss reaction (red dashed lines) has small time dependence and peaks in the late 21st century at ± 0.4 – 0.5% (for RCP8.5, the impacts are significantly larger as discussed below). For the Cl loss reaction, the global impact reflects that of the southern polar region (Figure 10) and follows the stratospheric chlorine loading with a maximum in the middle-late 1990s ($\pm 0.5\%$, ± 1.5 DU). As discussed above, the impact of the $\text{O}(^1\text{D})$ loss reaction has the opposite dependence on chlorine loading, as a slower (faster) $\text{O}(^1\text{D}) + \text{CH}_4$ reaction leads to more (less) ozone ($\pm 0.2\%$, ± 0.6 DU in the middle-late 1990s). The $\text{O}(^1\text{D})$ loss has the smallest impact of the three CH_4 loss processes.

Figure 11 (bottom) illustrates how these uncertainty ranges affect the overall rate of ozone change during 1960–2100 relative to the baseline and includes the effects of using different GHG scenarios. Ground-based ozone observations (symbols, updated from *Fioletov et al.* [2002]) are again shown for reference illustrating the range of observed interannual variability. All simulations have been offset to be zero in 1960 to emphasize the time dependence. For RCP4.5, the orange shading depicts the 2σ uncertainty range of the Cl loss uncertainty taken from Figure 11 (top) added to the baseline. As with SH polar ozone (Figure 10), this uncertainty range represents a modification of the rate of change in long-term global ozone decline and recovery. The slow uncertainty leads to a faster ozone decline during 1960–2000 and a faster recovery post-2000; the fast uncertainty leads to a slower decline and slower future recovery. Adding the $\text{O}(^1\text{D})$ loss uncertainty gives a slightly larger range (green shading), maximizing during times of highest chlorine loading (i.e., the slow $\text{O}(^1\text{D})$ and fast Cl uncertainty simulations are added for the combined positive ozone change, with the fast $\text{O}(^1\text{D})$ and slow Cl simulations added for the combined negative ozone change). Including the small time-dependent OH uncertainty effect to this range gives the absolute upper and lower

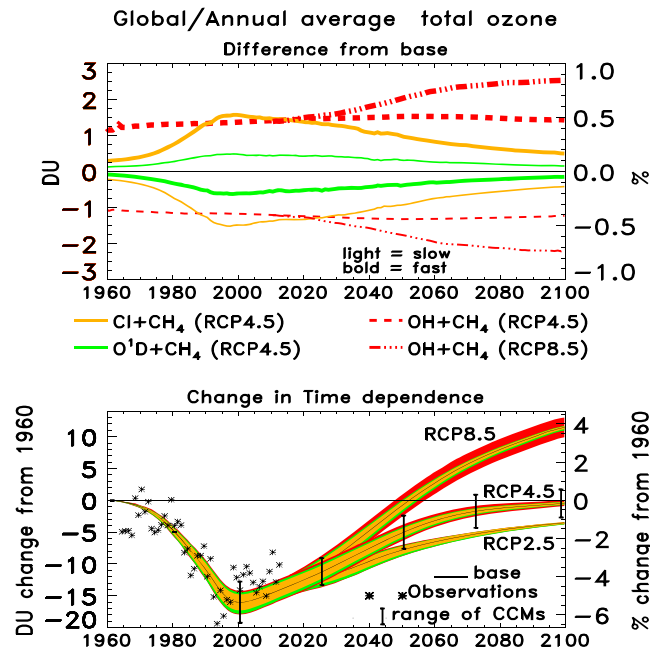


Figure 11. Time series of responses in global annual mean total column ozone due to uncertainties in the CH₄ loss reactions. (top) The 2σ uncertainty simulations plotted as the difference from the baseline using the RCP4.5 scenario and includes the OH loss reaction using RCP8.5 (red dash-dotted lines). The slow (fast) uncertainties are depicted by the light (bold) lines. (bottom) Changes in the time dependence: for RCP4.5, the range due to uncertainty in the Cl loss reaction from Figure 11 (top) is added to the baseline (orange shading); the range due to the combined uncertainties in the Cl and O^{(1)D} loss reactions from Figure 11 (top) are added to the baseline (i.e., the slow (fast) Cl and fast (slow) O^{(1)D} loss responses have been combined, green shading); and the range due to the combined uncertainties in the Cl, O^{(1)D} and OH loss reactions from Figure 11 (top) are added to the baseline (red shading). See text for details. The future response ranges using the RCP2.5 and RCP8.5 scenarios are also shown, and the baseline simulations for each RCP scenario are depicted by the black solid lines. All simulations have been offset to be zero in 1960 to emphasize the time dependence. Also shown are ground-based observations (symbols, updated from Fioletov et al. [2002]) and the range in chemistry-climate model simulations for selected years (vertical bars superimposed on the 2-D model RCP4.5 baseline) based on a subset of models shown to have realistic transport [Strahan et al., 2011].

+ CH₄ uncertainty response for RCP8.5 becomes increasingly larger through the 21st century (Figure 11, top), as does the combined uncertainty range (Figure 11, bottom). By 2100, the combined range for RCP8.5 is ±0.5% (±1.5 DU) relative to 1960. The substantial increase in the combined uncertainty ranges from RCP2.5 to RCP8.5 reflects the large range in CH₄ loading among the RCPs (1250–3750 ppb) and is driven mainly by uncertainty in the OH + CH₄ reaction (see also Table 4).

To add further perspective, the vertical bars show the approximate range in annual/global mean total ozone from chemistry-climate models for selected years, based on a subset of five models which were shown to have realistic transport as discussed in Strahan et al. [2011]. This represents the range of reasonable ozone values that would be expected based on the combined impacts of the individual model treatment of dynamics, chemistry, radiation, numerics, and other processes. For visual clarity, this range is superposed onto the 2-D model baseline simulation for RCP4.5. The range due to the combined CH₄ loss uncertainties is generally smaller than the multimodel range and becomes significantly smaller than the multimodel range for RCP2.5 and RCP4.5 in the late 21st century as chlorine loading diminishes.

limit impacts of all three CH₄ losses combined (red shading). Here the fast O^{(1)D} and slow Cl and OH loss uncertainties are added to the baseline to get the extreme negative ozone change, with the slow O^{(1)D} and fast Cl and OH loss uncertainties added to get the extreme positive ozone change. The combined uncertainty impact again strongly follows chlorine loading and is largest in the middle-late 1990s with a range of ±2.1 DU or ~±12% out of a baseline decline of 16 DU from 1960–2000. We note that these uncertainty ranges are essentially additive; i.e., simulations with all uncertainties combined give minimum/maximum ozone response ranges nearly identical to Figure 11 (bottom).

For future global ozone, the baseline simulations (black solid lines) show substantial range among the different RCP scenarios due to the very different GHG emissions, especially for CO₂ and CH₄. Baseline ozone amounts are largest for the RCP8.5 (high) scenario due to large CO₂ and CH₄ loading and are well above 1960 levels through the late 21st century. Similar responses in future tropospheric and stratospheric ozones among the RCPs were previously computed in 3-D CCMs [e.g., Kawase et al., 2011; Eyring et al., 2013]. For RCP4.5, the future CH₄ loss uncertainty ranges decrease through the 21st century following chlorine loading and are small by 2100. The uncertainty range diminishes at an even faster rate for the RCP2.5 (low) scenario. However, the OH

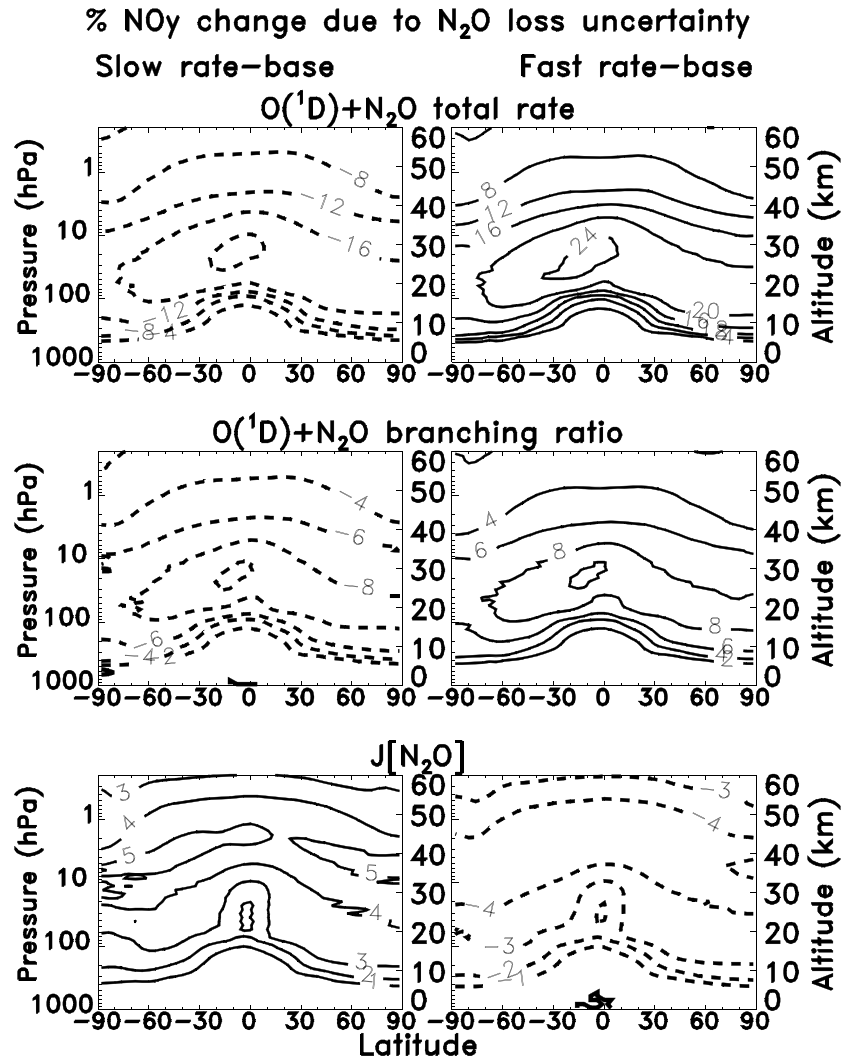


Figure 12. Percentage change in annual average total odd nitrogen (NO_y) for year 2000 due to the (left column) 2σ slow and (right column) 2σ fast uncertainties in the N_2O loss processes indicated. Changes are taken relative to the baseline. The contour intervals are (top row) $\pm 4\%$, (middle row) $\pm 2\%$, and (bottom row) $\pm 1\%$.

3.2.2. N_2O Loss Processes

As discussed in section 2.3 (Tables 1 and 2), the vast majority ($\sim 94\%$) of the loss of N_2O leads to the production of N_2 , with only $\sim 6\%$ of the loss producing odd nitrogen via reaction with $\text{O}(^1\text{D})$ (equations (R4a) and (R4b)). Uncertainty in the $\text{O}(^1\text{D})$ loss can have a substantial impact on stratospheric NO_x and total odd nitrogen (NO_y), and ozone, as was noted in the uncertainty analysis of *Considine et al.* [1999]. Figure 12 shows the present-day annual average NO_y changes due to both the overall rate uncertainty (Figure 12, top row) and the uncertainty in the branching ratio (Figure 12, middle row), which determines the amount of NO_x produced by this reaction. For the overall rate, the slow (fast) uncertainty yields substantial NO_y decreases (increases) throughout the upper troposphere and stratosphere, with maximum changes of $\pm 20\text{--}25\%$ in the tropical midstratosphere. The corresponding ozone changes are shown in Figure 13, with ozone increases (decreases) of 5–7% globally in the middle-upper stratosphere and polar lower stratosphere. The uncertainty in the $\text{O}(^1\text{D}) + \text{N}_2\text{O}$ branching ratio (Figures 12 and 13, middle rows) has a response that is qualitatively similar to the total rate uncertainty but with smaller magnitude, yielding maximum NO_y changes of $\pm 10\%$ and ozone changes of $\pm 2\text{--}3\%$. The uncertainty in N_2O photolysis ($\text{N}_2\text{O} + h\nu \rightarrow \text{N}_2 + \text{O}(^1\text{D})$; Figures 12 and 13, bottom rows) has the opposite impact on NO_y and ozone. Here slow photolysis yields NO_y increases (fast photolysis yields NO_y decreases) of up to 5% in the middle stratosphere. This is likely caused by the fact that slower

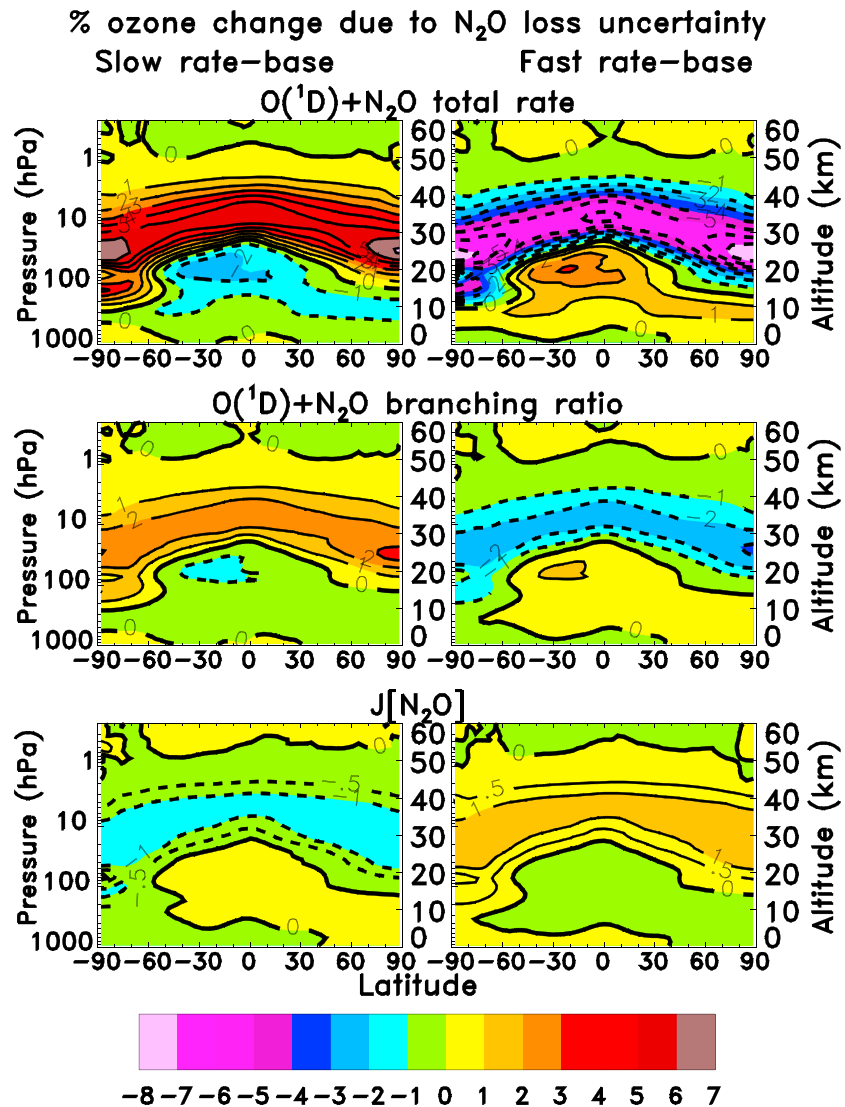


Figure 13. Percentage change in annual average ozone for year 2000 due to the (left column) 2σ slow and (right column) 2σ fast uncertainties in the N_2O loss processes indicated. Changes are taken relative to the baseline. The contour intervals are $\pm 1\%$ and include the $\pm 0.5\%$ contours.

N_2O photolysis leads to more N_2O available to react with $O(^1D)$, thereby enhancing the production of NO_y (with the opposite result caused by faster N_2O photolysis). This yields ozone decreases of $\sim 1\%$ in the middle stratosphere, with the opposite ozone response caused by faster N_2O photolysis (Figure 13, bottom row).

In addition to the primary ozone changes discussed above, uncertainty in the $O(^1D) + N_2O$ reaction also yields smaller ozone changes of opposite sign in the lowermost tropical stratosphere and upper troposphere (Figure 13, top and middle rows). Most of this is likely due to changes in the NO_x -ozone production cycle in this region: in the slow (fast) uncertainty case, reduced (enhanced) NO_x leads to less (more) ozone. A similar ozone response to N_2O perturbations was discussed in Revell *et al.* [2012]. Some of this ozone change also could be due to “self-healing,” wherein ozone decreases in the middle and upper stratosphere allow more solar UV radiation to penetrate to lower altitudes, leading to increased ozone production in the lower stratosphere (the reverse process occurs with ozone increases in the middle-upper stratosphere) [e.g., Mills *et al.*, 2008].

The 1960–2100 time series of the global total ozone impacts due to the N_2O loss processes are shown in Figure 14. Figure 14 (top) shows the difference of the uncertainty simulations from the baseline, with the

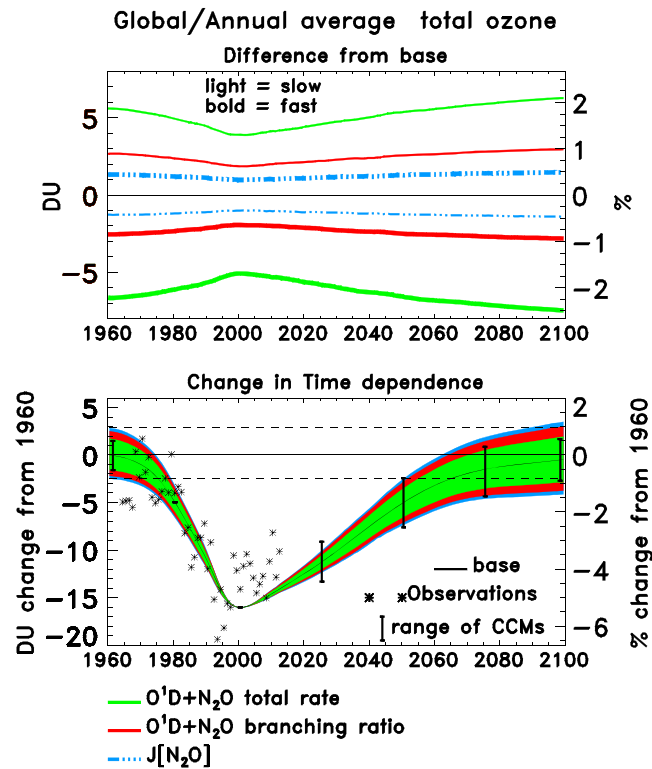


Figure 14. Time series of responses in global annual mean total column ozone due to uncertainties in the N_2O loss reactions. (top) The 2σ uncertainty simulations plotted as the difference from the baseline: the slow (fast) uncertainties are depicted by the light (bold) lines. (bottom) Changes in the time dependence: the range due to uncertainty in the total rate of the $O(^1D)$ loss reaction from Figure 14 (top) added to the baseline (green shading), the range due to the combined uncertainty in the total rate and branching ratio of the $O(^1D)$ loss reactions from Figure 14 (top) added to the baseline (red shading), and the range due to the combined uncertainty in the total rate and branching ratio of the $O(^1D)$ loss reaction and N_2O photolysis from Figure 14 (top) added to the baseline (i.e., the slow (fast) $O(^1D)$ loss and fast (slow) photolysis loss responses have been combined, blue shading). All simulations have been offset to be zero in 2000 to emphasize the time dependence. The dashed lines indicate the 1960 ozone amounts for the total combined upper and lower uncertainty simulations. See text for details. Also shown are the baseline simulation (black solid line), ground-based observations updated from Fioletov et al. [2002] (symbols), and the range in chemistry-climate model simulations for selected years (vertical bars superimposed on the 2-D model baseline), based on a subset of models shown to have realistic transport [Strahan et al., 2011].

ozone loss cycle and is largest during times of high chlorine loading. Also contributing to the time dependence is the increasing concentration of N_2O throughout the time period, which enhances the impact of the N_2O loss uncertainties. This effect is somewhat mitigated by the CO_2 induced stratospheric cooling, which increases the chemical loss of NO_x , as well as the strengthening of the Brewer-Dobson circulation [Rosenfield and Douglass, 1998; Plummer et al., 2010].

While the overall time dependence appears small compared to the larger absolute ozone changes shown in Figure 14 (top), the time dependence has a significant impact on the rate of ozone decline and recovery during 1960–2100 (Figure 14, bottom). Here the green shading depicts the range due to the $O(^1D)$ total rate uncertainty (2σ) from Figure 14 (top), added to the baseline. To emphasize the change in time dependence, this range has been offset to be zero in 2000, i.e., the year when the range is a minimum.

slow (fast) uncertainties depicted by the light (bold) lines. As reflected in Figure 13, a slower total rate and branching ratio for $O(^1D) + N_2O$, which create odd nitrogen, result in more global total ozone (light green and red lines); conversely, a faster total rate and branching ratio result in less ozone (bold green and red lines). During 1960–2100, the range in calculated ozone is largest for the total rate uncertainty (± 1.5 – 2.5%), with $\sim \pm 1\%$ for the branching ratio uncertainty. N_2O photolysis loss (blue dash-dotted lines) has a smaller and opposite effect as discussed above (Figures 12 and 13), with an uncertainty range in global total ozone of $\sim \pm 0.5\%$ throughout 1960–2100. As discussed in section 2.3, the uncertainty in N_2O photolysis is small given the level of agreement among laboratory measurements, and this is reflected in the small ozone response ranges in Figures 13 and 14.

Although the ozone responses due to uncertainties in the $O(^1D) + N_2O$ reaction are substantial and significantly larger than the CH_4 loss impacts (Figure 11), they represent a shift of the computed ozone time series by a mostly constant amount up or down from the baseline. However, another important factor is the change in the time dependence of the uncertainty impacts. Figure 14 (top) indicates that the ozone response to all of the N_2O loss processes is inversely correlated with the chlorine loading; i.e., the response is a minimum around year 2000. This is due to the fact that NO_x is sequestered in the reservoir species $ClONO_2$ via the $ClO + NO_2 + M \rightarrow ClONO_2 + M$ reaction. This process mitigates the odd nitrogen

The slow uncertainty calculation yields less NO_x to sequester chlorine in the reservoir ClONO_2 (i.e., more chlorine in radical forms), leading to faster ozone decline during 1960–2000. This combined with increasing N_2O loading leads to a faster recovery post-2000. Conversely, the fast uncertainty calculation leads to a slower pre-2000 ozone decline and slower recovery. These impacts are enhanced further by adding the branching ratio uncertainty to this range (red shading). This indicates that the combined uncertainty in the $\text{O}(^1\text{D}) + \text{N}_2\text{O}$ reaction represents a significant uncertainty in past and future model-computed ozone. By 2100, the combined uncertainty results in an ozone range of ± 1 –1.5% compared to 2000. Adding the small time-dependent N_2O photolysis uncertainty effect to this range gives the absolute upper and lower limit impacts of all N_2O loss processes combined (blue shading). Here the slow photolysis and fast $\text{O}(^1\text{D})$ loss uncertainties are added to the baseline to get the extreme negative ozone change, with the fast photolysis and slow $\text{O}(^1\text{D})$ loss uncertainties added to get the extreme positive ozone change. As with the methane losses, these N_2O loss uncertainty ranges are essentially additive, i.e., simulations with all uncertainties combined gives minimum/maximum ozone response ranges nearly identical to Figure 14 (bottom).

The vertical bars in Figure 14 show the approximate range from chemistry-climate models [Strahan *et al.*, 2011] superposed onto the 2-D model baseline as in Figure 11. By the late 21st century, the range due to the $\text{O}(^1\text{D}) + \text{N}_2\text{O}$ total rate uncertainty is comparable to the multimodel range, while the combined N_2O loss uncertainty range is notably larger than the multimodel range. Figure 14 (bottom) also shows that for the combined absolute positive response, ozone is projected to return to 1960 levels by ~ 2088 (upper dashed line), somewhat earlier than in the baseline simulation (~ 2100). However, for the combined absolute negative ozone response, return to 1960 levels is not projected to occur by year 2100 (lower dashed line). These results show that due to long-term changes in atmospheric chlorine and N_2O loading, uncertainties in the N_2O loss processes have significant impacts on past and future global ozone, including the projected date of return of future ozone to 1960 levels.

We found that future ozone responses to the N_2O loss uncertainties show only minor sensitivity to the GHG scenario, as indicated in Table 4 for 2100 (the values for RCP4.5 correspond to Figure 14, top). The response ranges are essentially the same for the low and medium scenarios (RCP2.5 and RCP4.5) and are actually slightly smaller for the high scenario (RCP8.5). This is due to the fact that while the N_2O surface concentration increases modestly ($\sim 25\%$) from RCP2.5 to RCP8.5 (344–434 ppb in 2100), CO_2 increases by more than a factor of 2 (421–931 ppm). The resulting increased CO_2 cooling of the stratosphere and enhanced stratospheric circulation in the higher scenario reduces the efficiency of the NO_x -ozone loss cycle [Rosenfield and Douglass, 1998; Plummer *et al.*, 2010], and this likely cancels and even slightly reverses any increased ozone response range caused by increased N_2O .

4. Conclusions and Future Directions

This study provides a detailed examination of the atmospheric loss processes of N_2O and CH_4 , their lifetimes, and the related impacts on ozone. Part of this study presents an overview of the work done in the recent SPARC lifetime report [SPARC, 2013], and additional details can be obtained from Chapter 3 of that report and the related supplements, as well as the NASA/JPL kinetic data evaluation. Here we provide a summary of the SPARC [2013] kinetic and photochemical evaluation and an analysis of the present-day and long-term ozone changes due to the estimated uncertainties in the N_2O and CH_4 loss parameters using 2-D and 3-D atmospheric model calculations.

Calculations from the 2-D model illustrate the vertical distribution of the different loss processes and their uncertainty ranges, along with the total global lifetimes. For N_2O , loss occurs in the stratosphere via UV photolysis in the 190–230 nm region and reaction with $\text{O}(^1\text{D})$. For CH_4 , the primary loss process is reaction with OH in the troposphere. Stratospheric loss due to reaction with OH, Cl, and $\text{O}(^1\text{D})$ makes a minor contribution to the total global lifetime of CH_4 . Photolysis at the hydrogen Lyman- α wavelength (121.567 nm) was found to be the dominant loss above 65–70 km for both N_2O and CH_4 , although this process has only a very minor impact on the total global atmospheric lifetime. Although the total global lifetimes of N_2O and CH_4 change very little between the JPL10-6 and the SPARC recommendations [SPARC, 2013], the 2σ uncertainty range is significantly reduced for the SPARC recommendations compared with JPL10-6: $\pm 6\%$ versus $\pm 11\%$ for N_2O and $\pm 13\%$ versus $\pm 25\%$ for CH_4 .

Model calculations show the magnitude of ozone responses due to 2σ uncertainties in the CH_4 and N_2O loss processes for present-day conditions, as well as the long-term changes (1960–2100). This represents uncertainty in calculated ozone due to input parameters that are common among models. For the uncertainty in the $\text{OH} + \text{CH}_4$ reaction rate coefficient, where the reaction impacts ozone mainly by the NO_x -ozone production cycle in the troposphere and lowermost stratosphere, the computed global total ozone response range (difference from the baseline) is ± 0.4 – 0.5% for present-day conditions. The response range due to the $\text{O}(^1\text{D})$ loss uncertainty is smaller (± 0.1 – 0.2%) and affects ozone via changes in the HO_x -ozone loss cycle in the upper stratosphere and by modulating the amount CH_4 available to react with Cl atoms in the SH polar lower stratosphere. The time dependence of the $\text{O}(^1\text{D})$ loss uncertainty range during 1960–2100 is small compared to the long-term changes in baseline global ozone. However, the time dependence of the OH loss uncertainty range is strongly dependent on the future CH_4 scenario: it is small for RCP2.5 (low) and RCP4.5 (medium) but is moderate for the RCP8.5 (high) scenario ($\pm 0.4\%$ in 2100 relative to 1960).

Reaction with Cl is a very minor loss process for CH_4 , accounting for $\sim 1.5\%$ of the total global loss. However, the 2σ uncertainty in this process has a modest impact on model-calculated ozone in the SH polar region and globally due to the conversion of chlorine from radical to reservoir forms and subsequent reduction in the chlorine catalyzed ozone loss. The ozone sensitivity to the $\text{Cl} + \text{CH}_4$ uncertainty in the SH polar region is somewhat mitigated by the reaction $\text{ClO} + \text{CH}_3\text{O}_2 \rightarrow \text{ClOO} + \text{CH}_3\text{O}$ along with the heterogeneous reaction $\text{HCl} + \text{HOCl} \rightarrow \text{Cl}_2 + \text{H}_2\text{O}$. For present-day levels of chlorine loading, both the 2-D model and GMI 3-D CTM compute total ozone ranges of ± 5 – 7% during the SH polar late winter-spring due to uncertainty in the $\text{Cl} + \text{CH}_4$ reaction rate coefficient. Some of this uncertainty is due to possible non-Arrhenius behavior of the $\text{Cl} + \text{CH}_4$ reaction at low temperatures characteristic of the polar lower stratosphere, which is not represented in the JPL10-6 recommendation. As a test of the model sensitivity to this behavior, the non-Arrhenius equation proposed by *Pilgrim et al.* [1997] was used in the 2-D and GMI models. This equation should be considered an upper limit of possible non-Arrhenius behavior that falls within the JPL10-6 uncertainty range and resulted in a total ozone increase of 4–5% in the ozone hole region for present-day chlorine loading. Overall, the current level of uncertainty in the $\text{Cl} + \text{CH}_4$ reaction has a moderate impact on the modeled ozone response in the SH polar region. A reduction in this uncertainty at low temperatures is desirable to refine the model ozone simulations.

Uncertainty in the parameters of the $\text{O}(^1\text{D}) + \text{N}_2\text{O}$ reaction, which leads to the production of stratospheric NO_x , has a significant impact on ozone via the NO_x -ozone loss cycle, NO_x participation in null cycles, and formation of NO_x -containing reservoirs. The 2σ uncertainty in the total rate coefficient of this reaction yields a substantial change in midstratospheric NO_y (± 20 – 25%) and global total ozone (± 1.5 – 2.5%) for present-day conditions. For the $\text{O}(^1\text{D}) + \text{N}_2\text{O}$ branching ratio uncertainty, which determines the amount of NO_x produced by this reaction, the global ozone response range is smaller but still significant ($\sim \pm 1\%$). Uncertainty in N_2O photolysis has the smallest ozone impact ($\sim \pm 0.5\%$) of the N_2O loss processes, given the overall good agreement among laboratory measurements. The ozone impact of this uncertainty is opposite to that of the $\text{O}(^1\text{D})$ loss: i.e., slower N_2O photolysis leads to less ozone as there is more N_2O available to react with $\text{O}(^1\text{D})$ allowing for increased production of stratospheric NO_x .

The responses to the N_2O loss processes are mostly constant in time, representing a shift in the ozone time series up or down from the baseline. However, there is a smaller but important time dependence in the responses that follows long-term increases in atmospheric N_2O loading and inversely follows chlorine loading. Combining the uncertainty impacts of all N_2O losses to get the absolute upper and lower limit ozone responses has a substantial effect on the rate of pre-2000 ozone decline and future recovery. The vast majority of this is due to uncertainty in the $\text{O}(^1\text{D})$ total reaction rate and branching ratio. The resulting uncertainty range in global total ozone increases throughout the 21st century and is ± 1 – 1.5% in 2100 relative to 2000. This also modifies the date of return of ozone to 1960 levels. For the combined absolute positive ozone response, return to 1960 levels occurs ~ 12 years earlier than the baseline. The ozone responses to the N_2O loss uncertainties revealed only minor sensitivity to future GHG scenarios, being slightly smaller for the high RCP8.5 scenario due to the mitigating impacts of the large CO_2 increases.

The global total ozone response ranges due the CH₄ and N₂O loss uncertainties were compared with the range of chemistry-climate model simulations shown to have realistic transport [Strahan *et al.*, 2011]. This multimodel range indicates the range of reasonable ozone values that would be expected based on the combined impacts of the individual model treatment of dynamics, chemistry, radiation, numerics, and other processes. While the ozone response ranges due to uncertainty in the CH₄ loss kinetics and N₂O photolysis were generally smaller than the multimodel range, the ranges due to uncertainty in the O(¹D) + N₂O reaction (total rate and branching ratio) were comparable to or larger than the multimodel range through the middle-late 21st century.

The results in this study suggest that uncertainty in current recommendations of the N₂O and CH₄ loss processes, which are used as inputs common among models, leads to significant uncertainty ranges in long-term model ozone simulations. The largest uncertainty ranges are due to the O(¹D) + N₂O reaction (both the total rate and branching ratio) and the Cl + CH₄ reaction, which is important in governing chlorine partitioning in the SH polar region. Reduction in the uncertainty of these reactions is desired to refine model ozone simulations.

Acknowledgments

We thank Susan Strahan and Steve Steenrod of the Global Modeling Initiative project for running the GMI CTM simulations used in this work. We also thank four anonymous reviewers for their helpful comments and suggestions. This work was supported in part by NOAA's Climate Goal and NASA's Atmospheric Composition Program. GSFC 2-D model output used in this manuscript will be provided to interested individuals upon request to E. Fleming (eric.i.fleming@nasa.gov).

References

- Amimoto, S. T., A. P. Force, R. G. Gulotty Jr., and J. R. Wiesenfeld (1979), Collisional deactivation of O(²D₂) by the atmospheric gases, *J. Chem. Phys.*, *71*, 3640–3647.
- Atkinson, R., D. L. Baulch, R. A. Cox, J. N. Crowley, R. F. Hampson, R. G. Hynes, M. E. Jenkin, M. J. Rossi, J. Troe, and T. J. Wallington (2008), Evaluated kinetic and photochemical data for atmospheric chemistry: Volume IV—Gas phase reactions of organic halogen species, *Atmos. Chem. Phys.*, *8*, 4141–4496.
- Bertrand, C., G. J. Collin, and H. Gagnon (1975), Coefficients d'absorption et rendements quantiques ioniques de composés inorganiques et d'hydrocarbures insaturés, *J. Chim. Phys.*, *72*, 719–723.
- Blitz, M. A., T. J. Dillon, D. E. Heard, M. J. Pilling, and I. D. Trought (2004), Laser induced fluorescence studies of the reactions of O(¹D₂) with N₂, O₂, N₂O, CH₄, H₂, CO₂, Ar, Kr and n-C₄H₁₀, *Phys. Chem. Chem. Phys.*, *6*, 2162–2171, doi:10.1039/b400283k.
- Bonard, A., V. Daële, J.-L. Delfau, and C. Vovelle (2002), Kinetics of OH radical reactions with methane in the temperature range 295–660 K and with dimethyl ether and methyl-*tert*-butyl ether in the temperature range 295–618 K, *J. Phys. Chem. A*, *106*, 4348–4389.
- Brasseur, G., and S. Solomon (2005), *Aeronomy of the Middle Atmosphere*, 3rd ed., Springer, Dordrecht, Netherlands.
- Bryukov, M. G., V. D. Knyazev, S. M. Lomnicki, C. A. McFerrin, and B. Dellinger (2004), Temperature-dependent kinetics of the gas-phase reactions of OH with Cl₂, CH₄, and C₃H₈, *J. Phys. Chem. A*, *108*, 10,464–10,472.
- Cantrell, C. A., R. E. Shetter, and J. G. Calvert (1994), Branching ratios for the O(¹D) + N₂O reaction, *J. Geophys. Res.*, *99*, 3739–3743, doi:10.1029/93JD02659.
- Carl, S. A. (2005), A highly sensitive method for time-resolved detection of O(¹D) applied to precise determination of absolute O(¹D) reaction rate constants and O(³P) yields, *Phys. Chem. Chem. Phys.*, *7*, 4051–4053, doi:10.1039/b513576c.
- Chan, W. F., G. Cooper, and C. E. Brion (1994), Discrete and continuum photoabsorption oscillator-strengths for the electronic spectrum of nitrous oxide (5.5–203 eV), *Chem. Phys.*, *180*, 77–88.
- Chipperfield, M. P., et al. (2014), Multi-model estimates of atmospheric lifetimes of long-lived ozone-depleting substances: Present and future, *J. Geophys. Res. Atmos.*, *119*, 2555–2573, doi:10.1002/2013J13JD021097.
- Considine, D. B., R. S. Stolarski, S. M. Hollandsworth, C. H. Jackman, and E. L. Fleming (1999), A Monte Carlo uncertainty analysis of ozone trend predictions in a two-dimensional model, *J. Geophys. Res.*, *104*, 1749–1765.
- Cox, R. A., R. G. Derwent, and P. M. Holt (1976), Relative rate constants for the reactions of OH radicals with H₂, CH₄, CO, NO and HONO at atmospheric pressure and 296 K, *J. Chem. Soc. Faraday Trans.*, *1*(72), 2031–2043.
- Crutzen, P. J. (1970), The influence of nitrogen oxides on the atmospheric ozone content, *Q. J. R. Meteorol. Soc.*, *96*, 320–325.
- Crutzen, P. J. (1971), Ozone production rates in an oxygen-hydrogen-nitrogen oxide atmosphere, *J. Geophys. Res.*, *76*, 7311–7327, doi:10.1029/JC076i030p07311.
- Crutzen, P. J., R. Muller, C. Bruhl, and T. Peter (1992), On the potential importance of the gas phase reaction CH₃O₂ + ClO → ClOO + CH₃O and the heterogeneous reaction HOCl + HCl → H₂O + Cl₂ in “ozone hole” chemistry, *Geophys. Res. Lett.*, *19*, 1113–1116, doi:10.1029/92GL01172.
- Davidson, J. A., H. I. Schiff, G. E. Streit, J. R. McAfee, A. L. Schmeltekopf, and C. J. Howard (1977), Temperature dependence of O(¹D) rate constants for reactions with N₂O, H₂, CH₄, HCl, and NH₃, *J. Chem. Phys.*, *67*, 5021–5025.
- Davidson, J. A., C. J. Howard, H. I. Schiff, and F. C. Fehsenfeld (1979), Measurements of the branching ratios for the reaction of O(¹D₂) with N₂O, *J. Chem. Phys.*, *70*, 1697–1704.
- Davis, D. D., S. Fischer, and R. Schiff (1974), Flash photolysis-resonance fluorescence kinetics study: Temperature dependence of the reactions OH + CO → CO₂ + H and OH + CH₄ → H₂O + CH₃, *J. Chem. Phys.*, *61*, 2213–2219.
- Dillon, T. J., A. Horowitz, and J. N. Crowley (2007), Absolute rate coefficients for the reactions of O(¹D) with a series of n-alkanes, *Chem. Phys. Lett.*, *443*, 12–16.
- Dillon, T. J., A. Horowitz, and J. N. Crowley (2008), The atmospheric chemistry of sulphuryl fluoride, SO₂F₂, *Atmos. Chem. Phys.*, *8*, 1547–1557.
- Douglass, A. R., M. R. Schoeberl, R. S. Stolarski, J. W. Waters, J. M. Russell III, A. E. Roche, and S. T. Massie (1995), Interhemispheric differences in springtime production of HCl and ClONO₂ in the polar vortices, *J. Geophys. Res.*, *100*, 13,967–13,978, doi:10.1029/95JD00698.
- Duncan, B. N., S. E. Strahan, Y. Yoshida, S. D. Steenrod, and N. Livesey (2007), Model study of the cross-tropopause transport of biomass burning pollution, *Atmos. Chem. Phys.*, *7*, 3713–3736, doi:10.5194/acp-7-3713-2007.
- Dunlea, E. J., and A. R. Ravishankara (2004), Kinetics studies of the reactions of O(¹D) with several atmospheric molecules, *Phys. Chem. Chem. Phys.*, *6*, 2152–2161.
- Dunlop, J. R., and F. P. Tully (1993), A kinetics study of OH radical reactions with methane and perdeuterated methane, *J. Phys. Chem.*, *97*, 11,148–11,150.

- Eyring, V., et al. (2013), Long-term ozone changes and associated climate impacts in CMIP5 simulations, *J. Geophys. Res. Atmos.*, *118*, 5029–5060, doi:10.1002/jgrd.50316.
- Finlayson-Pitts, B. J., M. J. Ezell, T. M. Jayaweera, H. N. Berko, and C. C. Lai (1992), Kinetics of the reactions of OH with methyl chloroform and methane: Implications for global tropospheric OH and the methane budget, *Geophys. Res. Lett.*, *19*, 1371–1374, doi:10.1029/92GL01279.
- Fioletov, V. E., G. E. Bodeker, A. J. Miller, R. D. McPeters, and R. Stolarski (2002), Global ozone and zonal total ozone variations estimated from ground-based and satellite measurements, *J. Geophys. Res.*, *107*(D2), 4647, doi:10.1029/2001JD001350.
- Fleming, E. L., C. H. Jackman, R. S. Stolarski, and A. R. Douglas (2011), A model study of the impact of source gas changes on the stratosphere for 1850–2100, *Atmos. Chem. Phys.*, *11*, 8515–8541, doi:10.5194/acp-11-8515-2011.
- Gierczak, T., S. Talukdar, S. Herndon, G. L. Vaghjani, and A. R. Ravishankara (1997), Rate coefficients for the reactions of hydroxyl radicals with methane and deuterated methanes, *J. Phys. Chem. A*, *101*, 3125–3134.
- Greenblatt, G. D., and A. R. Ravishankara (1990), Laboratory studies on the stratospheric NO_x production rate, *J. Geophys. Res.*, *95*, 3539–3547, doi:10.1029/JD095iD04p03539.
- Greiner, N. R. (1967), Hydroxyl-radical kinetics by kinetic spectroscopy. I. Reactions with H₂, CO, and CH₄ at 300°K, *J. Chem. Phys.*, *46*, 2795–2799.
- Hitchcock, V. C., E. Brion, and M. J. van der Wiel (1980), Absolute oscillator-strengths for valence-shell ionic photofragmentation of N₂O and CO₂ (8–75 eV), *Chem. Phys.*, *45*, 461–478.
- Howard, C. J., and K. M. Evenson (1976), Rate constants for the reactions of OH with CH₄ and fluorine, chlorine, and bromine substituted methanes at 296 K, *J. Chem. Phys.*, *64*, 197–202.
- Husain, D., J. M. C. Plane, and N. K. H. Slater (1981), Kinetic investigation of the reactions of OH(X²II) with the hydrogen halides, HCl, DCl, HBr and DBr by time-resolved resonance fluorescence (A²Σ⁺ – X²II), *J. Chem. Soc. Faraday Trans.*, *2*(77), 1949–1962.
- Jeong, K. M., and F. Kaufman (1982), Kinetics of the reaction of hydroxyl radical with methane and with nine Cl- and F-substituted methanes. 1. Experimental results, comparisons, and applications, *J. Phys. Chem.*, *86*, 1808–1815.
- Jonah, C. D., W. A. Mulac, and P. Zeglinski (1984), Rate constants for the reaction of OH + CO, OD + CO, and OH + methane as a function of temperature, *J. Phys. Chem.*, *88*, 4100–4104.
- Kawa, S. R., R. S. Stolarski, P. A. Newman, A. R. Douglass, M. Rex, D. J. Hofmann, M. L. Santee, and K. Frieler (2009), Sensitivity of polar stratospheric ozone loss to uncertainties in chemical reaction kinetics, *Atmos. Chem. Phys.*, *9*(22), 8651–8660, doi:10.5194/acp-9-8651-2009.
- Kawase, H., T. Nagashima, K. Sudo, and T. Nozawa (2011), Future changes in tropospheric ozone under Representative Concentration Pathways (RCPs), *Geophys. Res. Lett.*, *38*, L05801, doi:10.1029/2010GL046402.
- Madronich, S., and W. Felder (1985), Direct measurements of the rate coefficient for the reaction OH + CH₄ → CH₃ + H₂O over 300–1500 K 20th Int. Symp. Combustion 1984, 703.
- Margitan, J. J., F. Kaufman, and J. G. Anderson (1974), The reaction of OH with CH₄, *Geophys. Res. Lett.*, *1*, 80–81, doi:10.1029/GL001i002p00080.
- Matsumi, Y., K. Tonokura, Y. Inagaki, and M. Kawasaki (1993), Isotopic branching ratios and translational energy release of H and D atoms in reaction of O(¹D) atoms with alkanes and alkyl chlorides, *J. Phys. Chem.*, *97*, 6816–6821.
- Meinshausen, M., et al. (2011), The RCP greenhouse gas concentrations and their extensions from 1765 to 2300, *Clim. Change*, *109*, 213–241, doi:10.1007/s10584-011-0156-z.
- Mellouki, A., S. Téton, G. Laverdet, A. Quilgars, and G. Le Bras (1994), Kinetic studies of OH reactions with H₂O₂, C₃H₈ and CH₄ using the pulsed laser photolysis-laser induced fluorescence method, *J. Chim. Phys.*, *91*, 473–487.
- Mérienne, M. F., B. Coquart, and A. Jenouvrier (1990), Temperature effect on the ultraviolet absorption of CFCl₃, CF₂Cl₂ and N₂O, *Planet. Space Sci.*, *38*, 617–625.
- Mills, M. J., O. B. Toon, R. P. Turco, D. E. Kinnison, and R. R. Garcia (2008), Massive global ozone loss predicted following regional nuclear conflict, *Proc. Natl. Acad. Sci. U.S.A.*, *105*, 5307–5312.
- Morgenstern, O., G. Zeng, N. Luke Abraham, P. J. Telford, P. Braesicke, J. A. Pyle, S. C. Hardiman, F. M. O'Connor, and C. E. Johnson (2013), Impacts of climate change, ozone recovery, and increasing methane on surface ozone and tropospheric oxidizing capacity, *J. Geophys. Res. Atmos.*, *118*, 1028–1041, doi:10.1029/2012JD018382.
- Nishida, S., K. Takahashi, Y. Matsumi, N. Taniguchi, and S. Hayashida (2004), Formation of O(³P) atoms in the photolysis of N₂O at 193 nm and O(³P) + N₂O product channel in the reaction of O(¹D) + N₂O, *J. Phys. Chem. A*, *108*, 2451–2456.
- Oman, L. D., D. W. Waugh, S. R. Kawa, R. S. Stolarski, A. R. Douglass, and P. A. Newman (2010), Mechanisms and feedback causing changes in upper stratospheric ozone in the 21st century, *J. Geophys. Res.*, *115*, D05303, doi:10.1029/2009JD012397.
- Overend, R. P., G. Paraskevopoulos, and R. J. Cvetanovic (1975), Rates of OH radical reactions. I. Reactions with H₂, CH₄, C₂H₆, and C₃H₈ at 295 K, *Can. J. Phys.*, *53*, 3374–3382.
- Pilgrim, J. S., A. McLlroy, and C. A. Taatjes (1997), Kinetics of Cl atom reactions with methane, ethane, and propane from 292 to 800 K, *J. Phys. Chem. A*, *101*, 1873–1880.
- Plummer, D. A., J. F. Scinocca, T. G. Shepherd, M. C. Reader, and A. I. Jonsson (2010), Quantifying the contributions of stratospheric ozone changes from ozone depleting substances and greenhouse gases, *Atmos. Chem. Phys.*, *10*, 8803–8820, doi:10.5194/acp-10-8803-2010.
- Prather, M., C. Holmes, and J. Hsu (2012), Reactive greenhouse gas scenarios: Systematic exploration of uncertainties and the role of atmospheric chemistry, *Geophys. Res. Lett.*, *39*, L09803, doi:10.1029/2012GL051440.
- Prinn, R. G., et al. (2005), Evidence for variability of atmospheric hydroxyl radicals over the past quarter century, *Geophys. Res. Lett.*, *32*, L07809, doi:10.1029/2004GL022228.
- Revell, L. E., G. E. Bodeker, P. E. Huck, B. E. Williamson, and E. Rozanov (2012), The sensitivity of stratospheric ozone changes through the 21st century to N₂O and CH₄, *Atmos. Chem. Phys.*, *12*, 11,309–11,317, doi:10.5194/acp-12-11309-2012.
- Rienecker, M. M., et al. (2011), MERRA: NASA's Modern-Era Retrospective Analysis for Research and Applications, *J. Clim.*, *24*, 3624–3648.
- Rontu Carlon, N., D. K. Papanastasiou, E. L. Fleming, C. H. Jackman, P. A. Newman, and J. B. Burkholder (2010), UV absorption cross sections of nitrous oxide (N₂O) and carbon tetrachloride (CCl₄) between 210 and 350 K and the atmospheric implications, *Atmos. Chem. Phys.*, *10*, 6137–6149.
- Rosenfield, J. E., and A. R. Douglass (1998), Doubled CO₂ effects on NO_y in a coupled 2-D model, *Geophys. Res. Lett.*, *25*(23), 4381–4384, doi:10.1029/1998GL900147.
- Sander, S. P., et al. (2011), "Chemical kinetics and photochemical data for use in atmospheric studies, Evaluation Number 17", JPL Publication 10–6, Jet Propul. Lab., Pasadena, Calif. [Available at <http://jpldataeval.jpl.nasa.gov>]
- Selwyn, G. S., J. R. Podolske, and H. S. Johnston (1977), Nitrous oxide ultraviolet absorption spectrum at stratospheric temperatures, *Geophys. Res. Lett.*, *4*, 427–430, doi:10.1029/GL004i010p00427.

- Sharkey, P., and I. W. M. Smith (1993), Kinetics of elementary reactions at low temperature: Rate constants for the reactions of OH with HCl ($298 \geq T/K \geq 138$), CH₄ ($298 \geq T/K \geq 178$), and C₂H₆ ($298 \geq T/K \geq 138$), *J. Chem. Soc. Faraday Trans.*, *89*, 631–638.
- Stratospheric Processes and their Role in Climate (SPARC) (2013), SPARC report on the lifetimes of stratospheric ozone-depleting substances Their Replacements, and Related Species, M. Ko, P. Newman, S. Reimann and S. Strahan, SPARC Report No. 6, WCRP-15/2013.
- Spivakovsky, C. M., et al. (2000), Three-dimensional climatological distribution of tropospheric OH: Update and evaluation, *J. Geophys. Res.*, *105*, 8931–8980, doi:10.1029/1999JD901006.
- Strahan, S. E., B. N. Duncan, and P. Hoor (2007), Observationally derived transport diagnostics for the lowermost stratosphere and their application to the GMI chemistry and transport model, *Atmos. Chem. Phys.*, *7*, 2435–2445, doi:10.5194/acp-7-2435-2007.
- Strahan, S. E., et al. (2011), Using transport diagnostics to understand chemistry climate model ozone simulations, *J. Geophys. Res.*, *116*, D17302, doi:10.1029/2010JD015360.
- Sworski, T. J., C. J. Hohanadel, and P. J. Ogren (1980), Flash photolysis of H₂O vapor in CH₄. H and OH yields and rate constants for CH₃ reactions with H and OH, *J. Phys. Chem.*, *84*, 129–134.
- Takahashi, K., Y. Takeuchi, and Y. Matsumi (2005), Rate constants of the O(¹D) reactions with N₂, O₂, N₂O, and H₂O at 295 K, *Chem. Phys. Lett.*, *410*, 196–200.
- Tully, F. P., and A. R. Ravishankara (1980), Flash photolysis-resonance fluorescence kinetic study of the reactions OH + H₂ → H₂O + H and OH + CH₄ → H₂O + CH₃ from 298 to 1020 K, *J. Phys. Chem.*, *84*, 3126–3130.
- UNEP (2013), Drawing down N₂O to protect climate and the ozone layer A UNEP Synthesis Report.
- Vaghjiani, G. L., and A. R. Ravishankara (1991), New measurement of the rate coefficient for the reaction of OH with methane, *Nature*, *350*, 406–409.
- Vitt, F. M., and C. H. Jackman (1996), A comparison of sources of odd nitrogen production from 1974 through 1993 in the Earth's middle atmosphere as calculated using a two-dimensional model, *J. Geophys. Res.*, *101*, 6729–6739, doi:10.1029/95JD03386.
- Voulgarakis, A., et al. (2013), Analysis of present day and future OH and methane lifetime in the ACCMIP simulations, *Atmos. Chem. Phys.*, *13*, 2563–2587, doi:10.5194/acp-13-2563-2013.
- Vranckx, S., J. Peeters, and S. A. Carl (2008a), Absolute rate constant and O(³P) yield for the O(¹D) + N₂O reaction in the temperature range 227 K to 719 K, *Atmos. Chem. Phys.*, *8*(20), 6261–6272.
- Vranckx, S., J. Peeters, and S. Carl (2008b), A temperature dependence kinetic study of O(¹D) + CH₄: Overall rate coefficient and product yields, *Phys. Chem. Chem. Phys.*, *10*, 5714–5722.
- Wine, P. H., and A. R. Ravishankara (1982), O₃ photolysis at 248 nm and O(¹D₂) quenching by H₂O, CH₄, H₂, and N₂O: O(³P₂) yields, *Chem. Phys.*, *69*, 365–373.
- WMO (World Meteorological Organization), Scientific Assessment of Ozone Depletion (2007), Global Ozone Research and Monitoring Project-Rep., 50, 572 pp., Geneva, Switzerland.
- WMO (World Meteorological Organization), Scientific Assessment of Ozone Depletion (2011), Global Ozone Research and Monitoring Project-Rep., 52, 516 pp., Geneva, Switzerland.
- WMO (World Meteorological Organization), Scientific Assessment of Ozone Depletion (2014), Global Ozone Research and Monitoring Project-Rep., 55, 416 pp., Geneva, Switzerland.